The competing effects of wave amplitude and collisions on multi-ion-species suppression of stimulated Brillouin scattering in inertial confinement fusion hohlraums

R. L. Berger,* W. Arrighi, T. Chapman, and A. Dimits
Lawrence Livermore National Laboratory, P.O. Box 808, Livermore, California 94551, USA

J. W. Banks
Department of Mathematical Sciences, Rensselaer Polytechnic Institute, 301 Amos Eaton Hall, Troy, New York 12180, USA

S. Brunner
Centre de Recherches en Physique des Plasmas, Association Euratom-Confédération Suisse, Ecole Polytechnique Fédérale de Lausanne, CRPP-PPB, CH-1015 Lausanne, Switzerland

(Dated: March 7, 2023)

Reduction in stimulated Brillouin scattering (SBS) from National Ignition Facility hohlraums has been predicted through the use of multi-ion species materials on hohlraum walls. This approach to controlling SBS is based upon introducing a lighter ion species to the heavier ion species hohlraum wall in order to greatly increase the ion Landau damping of ion acoustic waves (IAWs). In a collisionless plasma, if the IAWs driven by SBS reach sufficient amplitudes, this increased damping is reduced or even eliminated by ion trapping in the IAWs. Here, the nonlinear behavior of IAWs is simulated with a multi-ion species Vlasov code including interspecies ion-ion collisions, self-collisions, and electron-ion pitch-angle collisions. The effect of collisions on the trapping of ions and electrons in a large-amplitude IAW is studied in a regime of relevance to current Inertial Confinement Fusion (ICF) experiments. Our simulations show that collisions can scatter trapped particles out of resonance with the IAW, suppressing trapping and helping to maintain an effective Landau damping of the IAW. The IAW amplitude required to trap particles in the presence of strong collisions is estimated analytically. These estimates are tested for strongly damped IAWs in tantalum oxide and pure helium plasmas. Our simulations show that, above a threshold amplitude, the damping is reduced by an amount inversely proportional to the wave amplitude. Thus, the success of controling SBS using multispecies plasma may depend sensitively on laser power and pulse length.

I. INTRODUCTION

In the past few years, indirectly driven deuterium-tritium (DT) implosion experiments on the National Ignition Facility (NIF) have increased the maximum neutron yield by orders of magnitude[1–3] without radical changes in hohlraum and capsule design nor in laser delivery. This result might indicate that the system is at a threshold's edge such that an increase in laser power and energy would allow entry into a robust above-ignition-threshold regime where exciting new physics results await. Increases in power and energy mean higher risks that Laser Plasma Interaction (LPI) thresholds will be exceeded. The high performing Diamond shots in 2017[4–6] had modest stimulated Brillouin scatter (SBS) but similar high performing BigFoot shots in 2018 had significant SBS.[7] The Hybrid-E designs[8] with record yield have not experienced high levels of SBS to date. These designs, all with gold or uranium walls and 0.3 mg/cc helium fills, ablated high-Z plasma from the walls that, in some cases, provided fertile ground for Brillouin scatter of large fractions of laser energy. More recent record yield experiments using cross beam energy transfer have resulted in negligible SBS as a result of transferring energy from the outer to inner beams.[9]

SBS is a three wave resonant instability where the ponderomotive force of a backscattered light wave and the incident laser light drive resonantly an ion acoustic wave (IAW) that itself backscatters the laser light. If the IAW damping is small enough and plasma gradients are weak enough, this interaction grows exponentially.

The risk of high levels of SBS was recognized early in the indirect drive Inertial Confinement Fusion (ICF) program with possibly high SBS for the outer cone of beams (angles of 44-52 degrees with respect to the hohlraum axis) and less for the inner cone (angles of 23-30 degrees with respect to the hohlraum axis).[10] Two-thirds of the beams and thus two-thirds of the maximum laser power and energy are delivered by the outer beams. A method to reduce the risk of high SBS in National Ignition Facility (NIF) ignition hohlraums was proposed and employed in the first years of NIF shots, namely adding a $1\mu m$ gold-boron layer to the inside surface of the hohlraum wall such that the laser interacted with a two-ion-species plasma with strong IAW damping instead of a pure high-Z plasma with weak damping.[11] The initial ICF designs pursued high capsule gain which required long laser pulses ($\sim 18-20$ ns) and high fill gas density (~ 1 mg/cc). Contrary to design expectations, the initial capsule implosions were very asymmetric. Obtaining symmetry required the transfer of large

* Berger5@llnl.gov

fractions of laser energy away from the outer beams that interacted with the high-Z plasma to the inner beams that interacted with the He and CH plasma ablated from the capsule shell. As a consequence, stimulated Raman rather than Brillouin scatter became the LPI problem to control. Thus, the practice of adding boron to gold was abandoned after it was established that SBS was small in these modified designs, even with pure gold walls.

The early designs were unsuccessful in achieving the promised high capsule gain because of hydrodynamic problems that degraded the capsule yield.[12] Subsequently, designs with more robust performance that used shorter laser pulses (~ 14 ns) and fill gas densities ~ 1.6 mg/cc were successfully pursued.[13] Eventually, designs with pulse durations as short as 6 ns and He fills as low as 0.3 mg/cc that required high density carbon (HDC) capsules were successful in producing neutron yields in excess of 10^{16}. In addition, little to no transfer of laser energy was required to achieve symmetry which allowed the full use of the power and energy of the NIF. Other gas fill densities were used such as 0.6 mg/cc, 0.45 mg/cc and the near vacuum hohlraums with 0.03 mg/cc. Reference 14 provides detailed comparison of the indirect drive designs that are beyond the scope of this work.

In 2017-2019, experiments with high power ($\sim 400-500$ TW, thus 10 TW per NIF Quad) and energy (~ 2 MJ)) that demonstrated high yield raised concerns that laser mirror damage was likely with this design. The SBS from this series of shots was well reproduced with the laser plasma interaction code pF3D[7]. In the aftermath of these shots, pF3D simulations were done to show SBS in those and similar designs could be greatly reduced by ultilizing a tantalum-oxide (Ta_2O_5) liner on the inside surface of the hohlraum wall.[7, 15] More recent experiments with Ta_2O_5 with modest laser power and energy were successful in nearly eliminating SBS in hohlraums.[16] The performance of Ta_2O_5 at nearly full NIF power and energy has not yet been tested.

The Laser MegaJoule (LMJ)[17, 18] is designed to have nearly the same maximum power and energy as NIF. However, the spotsize at best focus is significantly smaller than NIF's which results in a higher intensity than at the NIF for the same beam power. For the outer cone of beams, the average laser intensity for a NIF outer quad power of 10TW is $\sim 1.6\times10^{15}\mathrm{W/cm^2}$ but twice that for LMJ with a spot size one-half of NIF. Use of materials like Ta_2O_5 to control SBS may be more imperative for LMJ.

In a pure gold or uranium plasma, the ion acoustic wave is very weakly Landau damped because the phase velocity, $v_{ph} \approx \sqrt{Z_{Au}T_e/M_{Au}}$, is much larger than the ion thermal velocity, $\sqrt{T_{Au}/M_{Au}}$. Here, Z_{Au} is the charge state of gold ions, T_e is the electron thermal velocity, M_{Au} is the mass of gold ions, and T_{Au} is the temperature of the gold plasma. Because of this weak damping, the growth rate of SBS can be high enough to scatter large amounts of laser light. Adding light ions changes the phase velocity but significant ion damping can occur if the phase velocity is similar to the light ion thermal velocity, that is $v_{ph} \sim \sqrt{T_B/M_B}$, where T_B is the temperature of the boron plasma, and M_B is the mass of boron ions. Here, $T_B \sim T_{Au}$ but $M_{Au}/M_B \approx 18$.

One concern with this technique is that the IAW will grow to sufficient amplitude to trap the light ions and reduce or eliminate the additional damping provided by the light ions; that is, 'kinetic inflation' will occur, again permitting high levels of SBS.[19] In the absence of particle collisions, we expect inflation will occur if the particles, trapped by the wave at the phase velocity of the wave, execute a bounce oscillation before the wave is Landau damped, that is, $\omega_{bj}/\gamma_L \gg 1$. The IAW Landau damping rate for a Maxwell-Boltzmann distribution of electrons and ions is γ_L, and the bounce frequency of deeply trapped particles is $\omega_{bj} = k\sqrt{e|Z_j|\phi/m_j}$, k is the wavenumber of the IAW, and the half-width of the trapping region in velocity is $\Delta v_{tr,j} = 2\sqrt{|Z_j|e\phi/m_j}$ where ϕ is the electrostatic potential of the IAW, $Z_e = -1$ and $m_j = A_j m_p$ for $j \neq e$ where m_p is the proton mass and A_j is the atomic mass number for species,'j'.

In our study where the wave is driven over many periods, trapping will occur, especially for the electrons with fast bounce frequencies.[20] However, collisions act to detrap particles before they can execute a bounce especially in the case considered here of electrons and light ions colliding with heavy, high-Z ions. A study of SBS in two-ion species plasma with ion-ion collisions with a hybrid particle-in-Cell code demonstrated that collisions act to maintain a negative slope to the distribution function in the trapping region of velocity space.[21] In the Appendix of Reference 20, collisional detrapping conditions were given for electrons and ions in a single ion species plasma. Here, using the same techniques established there, we easily generalize these estimates to two-ion species plasmas in Sec. II. In Sec. III, we use one spatial and two velocity dimension (1D+2V) Vlasov simulations to test collisional effects on trapping and wave damping. Pitch-angle and self-collision operators were added to LOKI and used in recent publications.[22, 23] Interspecies collisions were added recently.[24] LOKI is a 4D (2D-2V) multispecies Eulerian Vlasov code that employs 6th-order conservative finite differences for the spatial discretization, and 6th-order accurate Runge Kutta time stepping. The implementation is highly scalable using MPI parallelism, and is routinely run on thousands or tens-of-thousands of processors.[25, 26] We find that collisional de-trapping maintains the Landau damping of the light ions but with a reduced damping rate that depends on the wave amplitude but is still more than an order of magnitude larger than the damping in pure gold or uranium. As the dissipation is maintained, heating of all three species also continues whereas the time-averaged heating and damping ceases without collisions.

In the collisionless case, large-amplitude, BGK-type nonlinear waves can be created and persist over many bounce periods because of the absence of damping. These states have been shown to be unstable to res-

onant instabilities and filamentation-like or modulational instabilities[27–31]. Recently, multi-dimensional particle-in-cell simulations of SBS showed that IAW filamentation, caused by trapped ion induced wavefront bowing, dominated the saturation of SBS in a Nitrogen plasma over a range of ZT_e/T_i.[32] In Sec. IV, we show with 2D+2V Vlasov simulations that, although collisions are significant, this instability persists as in the work of Albright *et al.*[32] but does not determine the maximum wave amplitude and develops only after the ponderomotive drive is turned off. With and without collisions the wave damping rate is very small. However, for Ta_2O_5 plasmas where the IAW is strongly damped, this instability did not occur. We conjecture that many of the instabilities that rely on the presence of a population of trapped particles will be stabilized when the de-trapping conditions are met. In Sec. V, the energy conservation and the heating of each plasma species is discussed with and without collisions for single-ion helium plasma and two-ion Ta_2O_5 plasmas. In Sec. VI, we summarize our results and speculate on their implications for other laser plasma instabilities.

II. THEORY

The linear kinetic theory of the frequency and damping of IAW with multiple ion species for collisionless plasma has been explored in some detail for low-Z plasmas and for high-Z plasmas with low mass ions added.[11] Because of their common use in laser plasma interaction experiments, hydrocarbons, *e.g.* $CH, CH_4, C_3H_8, C_5H_{12}$, received special attention. In general, there are two least damped modes for hydrocarbons. If $T_e/T_i \gg 10$, the least damped mode, often called the fast wave, has a phase velocity, $v_{\rm ph}$, greater than the thermal velocity of both ion species. Most of the Landau damping is from the protons with its unique $Z/A = 1$. If $T_e \sim T_i$, this fast wave is strongly damped, and the slow wave is the least damped wave with a phase velocity intermediate between the two ion thermal velocities, $\sqrt{\rm T_i/m_c} < {\rm v_{ph}} \lesssim \sqrt{\rm T_i/m_p}$ where $\rm m_c$, $\rm m_p$ is the carbon, proton mass respectively. Because these masses are not very different, the slow mode for hydrocarbons is also strongly damped. Kinetic Vlasov simulations studied the frequency and damping of nonlinear IAWs in CH plasmas.[33] The mass ratio might be much larger, *e.g.* 200, if protons could be added to gold but practically beryllium (Z=4, A=9) is the lowest possible mass that could be mixed with gold. Boron was initially chosen for experiments because of the health risks associated with manufacturing with beryllium and restrictions on introducing beryllium to the experimental facility.

For plasmas composed of high-Z, high-mass ions and low-Z, light ions, collisions cannot be ignored in choosing realistic values for the plasma parameters, $\rm T_e, T_i$, and $\rm n_e$. Furthermore, the slow mode essentially does not exist if collisional drag is taken into account.[34] Tantalum-oxide, Ta_2O_5, is interesting as a hohlraum wall liner material because it provides strong Landau damping of IAWs while sacrificing little radiation flux compared to pure gold and because it can be made into a low density foam that could be used to control radiation symmetry. Ref. 7 used pF3D simulations to show Ta_2O_5 and AuB were equally effective in controlling SBS. Those simulations assumed that the Landau damping of the IAW was unaffected by the amplitude of the wave because of the strong pitch-angle collisions of the electrons and oxygen ions on the highly ionized gold ions and the strong self-collisions of the gold ions. That assumption is examined here with 1D+2V Vlasov simulations of propagating IAWs. The plasma considered is stationary partially ionized tantalum and fully ionized oxide with (Z=50,8) and (A=181,16) and with $n_e = 0.05n_c$ and $T_e = T_i = 5$ keV where n_c is the critical density of 351nm light. Solving the linear kinetic dispersion relation for pure tantalum, the complex frequency is $\omega/\omega_{pe} = (0.8453 - 0.002653i) \times 10^{-2}$, a very weakly damped IAW. Setting $\omega_r = Re(\omega)$ and $\gamma = Im(\omega)$, the ratio of the damping rate to the real frequency is $\gamma/\omega_r = 3.14 \times 10^{-3}$ for pure tantalum. Note, $\omega_{pe} = 1.19886 \times 10^{15}{\rm sec}^{-1}$ and $k\lambda_{De} = 0.86$ where k is the wavenumber of the IAW. For Ta_2O_5, $\omega/\omega_{pe} = (1.137 - 0.2414i) \times 10^{-2}$, $\gamma/\omega_r = 0.212$, a very strongly damped IAW.

Because the hohlraum interior is typically filled with helium gas both to cool the DT fuel in the capsule and to slow down the expansion of the high-Z wall into the path of the laser beams, we briefly consider the effect of collisions on the trapping of ions. For pure helium with $n_e = 0.05n_c$, $T_e = 2T_i = 4$ keV, Z=2, and A=4, the IAW frequency and damping rate are $\omega/\omega_{pe} = (1.602 - 0.3123i) \times 10^{-2}$, that is, $\gamma/\omega_r = 0.195$, a very strongly damped IAW for a Maxwell-Boltzman ion distribution.

In general, three collisional dynamics effects may lead to detrapping: (1) Slowing-down (drag), (2) parallel diffusion, and (3) transverse diffusion (pitch-angle scattering). For collisions of species a on species b, assumed to be at thermal equilibrium and represented by a Maxwellian distribution with density N_b and temperature T_b, these effects are represented by the relations [35],[36]:

$$\frac{d}{dt}\langle \mathbf{v} \rangle = -\nu_s^{ab}\, \mathbf{v}, \tag{1}$$

$$\frac{d}{dt}\langle (\mathbf{v}_\parallel - \langle \mathbf{v}_\parallel \rangle)^2 \rangle = \nu_\parallel^{ab}\, v^2, \tag{2}$$

$$\frac{d}{dt}\langle (\mathbf{v}_\perp - \langle \mathbf{v}_\perp \rangle)^2 \rangle = \nu_\perp^{ab}\, v^2, \tag{3}$$

where $\langle . \rangle$ stands for a statistical average over a set of particles a, all with the same incoming velocity $\mathbf{v}$ of norm v. The subscripts $\parallel$ and $\perp$ respectively refer to the directions parallel and perpendicular to $\mathbf{v}$.[37] The collision

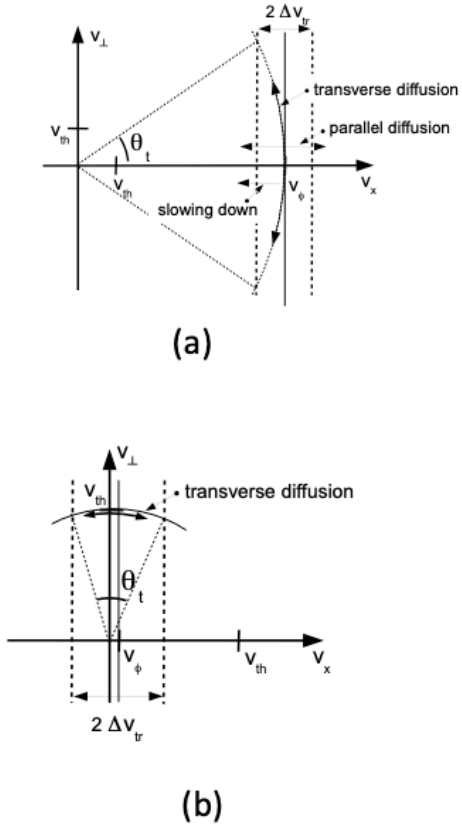

FIG. 1: (a) Detrapping in the tail of the distribution applicable to resonant light ions in a two-ion-species IAW (b) Detrapping in the bulk of the distribution applicable to resonant electrons in an IAW. Here, $v_\phi = v_{\rm ph}$. Reproduced from Physics of Plasmas **20**, 0321107 (2013); https://doi.org/10.1063/1.4794346, with permission of AIP Publishing.

rates appearing in Eqs. (1)-(3) are given by

$$\nu_s^{ab}(v)/\nu_c^{ab}(v) = (1+\frac{m_a}{m_b})\,\psi(x^{ab}), \tag{4}$$

$$\nu_\parallel^{ab}(v)/\nu_c^{ab}(v) = \frac{\psi(x^{ab})}{x^{ab}}, \tag{5}$$

$$\nu_\perp^{ab}(v)/\nu_c^{ab}(v) = 2\left[\left(1-\frac{1}{2x^{ab}}\right)\,\psi(x^{ab})+\psi'(x^{ab})\right], \tag{6}$$

where $\psi(x) = -(2/\sqrt{\pi})\sqrt{x}\exp(-x) + \mathrm{erf}(\sqrt{x})$, $\mathrm{erf(x)} = (2/\sqrt{\pi})\int_0^x \exp(-t^2)dt$, and $\psi'(x) = d\psi/dx = (2/\sqrt{\pi})\sqrt{x}\exp(-x)$ with argument $x^{ab} = m_b v^2/2T_b = v^2/2v_{\rm th,b}^2$. The basic collision frequency ν_c^{ab} appearing in Eqs. (4)-(6) is given by

$$\nu_c^{ab}(v) = \frac{q_a^2 q_b^2 \log\Lambda_{ab} N_b}{4\pi\epsilon_0^2 m_a^2 v^3}, \tag{7}$$

where ϵ_0 is the permittivity of free space, $q_s = Z_s e$ is unsigned charge on species 's=a,b' with charge state Z_s, N_b is the density of species 'b', and the $\log\Lambda_{ab}$ stands for the collision logarithm.

Our focus is on the interplay of trapping and collisions in multi-ion species plasmas. Ion trapping occurs for velocities $v_{\rm ph} - \Delta v_{\rm tr,i} < v_x < v_{\rm ph} + \Delta v_{\rm tr,i}$, which lies is in the tail of the ion distribution (see Fig. 1a). The IAW propagates in the x-direction. For IAWs of interest (i.e., those that are weakly through to strongly damped, but not so strongly damped that they are unable to participate in SBS), the real frequency of the fast mode (or the least damped mode in a single-ion-species IAW) is reasonably approximated[11] as,

$$\omega = kC_s, \tag{8}$$

$$C_s = \sqrt{(Z/A)_{\rm eff}\frac{T_e}{m_p(1+k^2\lambda_{De}^2)}}, \tag{9}$$

$$(Z/A)_{\rm eff} = \frac{\sum_i f_i \frac{Z_i^2}{A_i}}{\sum_i f_i Z_i}, \tag{10}$$

where λ_{De} is the electron Debye length, f_i is the atomic fraction of each ion species. $v_{\rm thi,i} = \sqrt{T_i/m_i}$ is the thermal velocity of the i$^{\rm th}$ ion species. Applying this to Ta_2O_5, we find $(Z/A)_{\rm eff} = 0.34$, $v_{\rm ph}/v_{\rm thi,i} \simeq \omega/(kv_{\rm thi,i}) = 0.58((A_iT_e/T_i)/(1+k^2\lambda_{De}^2))^{1/2} = [5.92, 1.76]$ and $\Delta v_{\rm tr,i}/C_s = [1.37, 1.84](e\phi/T_e)^{1/2}$, so that in this case, the ordering $v_{\rm ph} \simeq C_s \gtrsim v_{\rm thi,O}$ and $v_{\rm ph} \gg v_{\rm thi,Ta}, \Delta v_{\rm tr,Ta}, \Delta v_{\rm tr,O}$ applies. In the previous sentence, the first term in square brackets applies to tantalum ions and the second to oxygen ions.

As shown in Fig. 1a, collisions lead to ion detrapping by parallel and transverse diffusion (pitch-angle scattering) as well as slowing down (drag). The change in trapped ion velocity has to be enough that the velocity parallel to the wave propagation direction, v_x in this case, falls outside the trapping region. In transverse diffusion for example, the angle required is much less than 90° because $\Delta v_{\rm tr,i}/v_{\rm ph} \ll 1$. Because of the higher charge state of the heavier ion species, the detrapping of the lighter ion species is dominated by collisions from the heavier ion collisions rather than self collisions [c.f. Eq. (7)]. The electron contribution to ion detrapping is negligible primarily because of the species mass ratio. The ordering of ion velocities means that the characteristic velocity of trapped ions is $v_{\rm ph}$. Setting a=O and b=Ta in Eqs. (4-6), one finds $x^{\rm OTa}(v_{\rm ph}) \gg 1$ and therefore $\psi[x^{\rm OTa}(v_{\rm ph})] \simeq 1$ and $\psi'[x^{\rm OTa}(v_{\rm ph})] \ll 1$, yielding $\nu_s^{\rm OTa}(v_{\rm ph}) \simeq \nu_c^{\rm OTa}(v_{\rm ph})$, $\nu_\parallel^{\rm OTa}(v_{\rm ph}) \simeq 2(v_{\rm th,Ta}/v_{\rm ph})^2\nu_c^{\rm OTa}(v_{\rm ph})$, and $\nu_\perp^{\rm OTa}(v_{\rm ph}) \simeq 2\nu_c^{\rm OTa}(v_{\rm ph})$.

Collisional detrapping of oxygen ions requires the collisional timescales $\tau_{s,||,\perp}^{OTa}$ to be competitive with the ion bounce period. Together, Eqs. (1-3) and Fig. 1a yield the collisional timescales,

$$\tau_s^{\rm OTa} = \frac{\Delta v_{\rm tr,O}}{v_{\rm ph}} \frac{1}{\nu_s^{\rm OTa}(v_{\rm ph})}, \tag{11}$$

$$\tau_{||}^{\rm OTa} = \left(\frac{\Delta v_{\rm tr,O}}{v_{\rm ph}}\right)^2 \frac{1}{\nu_{||}^{\rm OTa}(v_{\rm ph})}, \tag{12}$$

$$\tau_{\perp}^{\rm OTa} = \frac{\theta_t^2}{\nu_{\perp}^{\rm OTa}(v_{\rm ph})} \tag{13}$$

$$\simeq \frac{2\Delta v_{\rm tr,O}}{v_{\rm ph}} \frac{1}{\nu_{\perp}^{\rm OTa}(v_{\rm ph})}, \tag{14}$$

where for $\tau_{\perp}^{\rm OTa}$ we have used $1-\cos(\theta_t) \simeq \theta_t^2/2$. Setting the requirement for effective detrapping $\omega_{b,\rm O}\tau_{s,||,\perp}^{\rm OTa} \lesssim 2\pi$, we find the the approximate detrapping thresholds,

$$\frac{e\phi}{T_e} < \pi\sqrt{\frac{T_i}{Z_{\rm O}T_e}} \frac{v_{\rm ph}}{v_{\rm th,O}} \frac{\nu_c^{\rm OTa}}{kC_{\rm s,O}}, \tag{15}$$

for transverse diffusion or slowing down (the thresholds are the same, as detailed in Ref. 20), and,

$$\frac{e\phi}{T_e} < \left(\pi \frac{T_i}{Z_{\rm O}T_e} \frac{m_{\rm O}}{m_{\rm Ta}} \frac{\nu_c^{\rm OTa}}{kC_{\rm s,O}}\right)^{2/3}, \tag{16}$$

for parallel diffusion, where $C_{\rm s,O} = \sqrt{Z_{\rm O}T_e/m_O}$. Which threshold is the more stringent depends on parameters; in the case considered here, transverse diffusion and slowing down are the more effective detrapping mechanisms with a threshold on ϕ greater by a factor of 2 than for parallel diffusion, while for a single ion species, parallel diffusion is typically dominant[20].

Finally, the contribution of the electrons to the linear Landau damping of the IAW is small, but we consider their trapping and detrapping because of their role in self-focusing (discussed later). Electron trapping occurs for velocities $v_{\rm ph} - \Delta v_{\rm tr,e} < v_x < v_{\rm ph} + \Delta v_{\rm tr,e}$ that lie in the bulk of the distribution (see Fig. 1b) because one has the velocity ordering $v_{\rm ph} \ll v_{\rm the}$ and $\Delta v_{\rm tr,e}/v_{\rm the} = 2\sqrt{e\phi/T_e} \ll 1$. This velocity ordering means that the characteristic velocity of electrons scattering from the trapped region is the transverse thermal velocity, $v_{\rm the}$, and only transverse diffusion is effective at scattering electrons from the trapped region, shown in Fig. 1b (parallel diffusion and slowing down cannot effetively scatter electrons from the trapped region). Transverse diffusion has contributions from electron self collisions and electron-ion collisions from both ion species, but in the limit $Z \gg 1$ will be dominated by the ions and specifically the heavier (higher-charge) ion species [c.f. Eq. (7)].

Similar to the ion case, one finds for the electrons, $x^{ei}(v_{\rm the}) \gg 1$ and therefore $\psi[x^{ei}(v_{\rm the})] \simeq 1$ and $\psi'[x^{ei}(v_{\rm the})] \ll 1$, giving $\nu_{\perp}^{\rm ei}(v_{\rm the}) \simeq 2\nu_c^{ei}(v_{\rm the})$. Equation. (3) and Fig. 1b yield $\tau_{\perp}^{ei} \approx \theta_t^2/\nu_{\perp}^{ei}(v_{\rm the}) \approx (\Delta v_{\rm tr,e}/v_{\rm the})^2/\nu_{\perp}^{ei}(v_{\rm the})$. Applying the criterion, $\omega_{b,e}\tau_{\perp}^{ei} < 2\pi$, for collisional detrapping to be significant, we estimate the electron detrapping threshold to be,

$$\frac{e\phi}{T_e} < \left(\frac{\pi}{k\lambda_{ei}(v_{\rm the})}\right)^{2/3}, \tag{17}$$

for which $\lambda_{ei} = v_{\rm the}\tau_{\perp}^{ei}$ is the electron-ion scattering mean free path.

The electron-ion collision rate for the case studied here is 1.1×10^{12} sec^{-1}. The collision rate of a thermal oxygen ion from tantalum is 1.5×10^{11} sec^{-1} and 1.3×10^{10} sec^{-1} at the phase velocity. The oxygen ion self collision rates are an order of magnitude slower. Evaluating the thresholds for the chosen Ta_2O_5 plasma, we find the threshold in wave amplitude $\delta n/n_e \simeq e\phi/T_e$ for oxygen ion detrapping to be 1.8×10^{-3} and for electron detrapping 2.3×10^{-2}. i.e., the wave amplitude required to trap electrons is an order of magnitude larger than that required to trap oxygen ions.

III. SIMULATIONS OF DE-TRAPPING

In this section, LOKI simulations are used to examine the effect of collisions on de-trapping ions and electrons and on the damping rates of the IAWs for both single and multiple ion species plasma. The IAW amplitudes of interest to kinetic simulations of nonlinear processes in ICF hohraum plasmas are estimated by using pF3D[38] simulations of SBS in Ta_2O_5 plasma with the same temperatures and ionization states used in Sec II. [39]

In addition to LOKI simulations of Ta_2O_5 plasma presented in Sec.III B 1, LOKI simulations for helium plasma which is the standard material used to fill the hohlraum interior, and for nitrogen plasma (used for basic physics experiments of SBS and in the PIC simulations of those experiments[32]) were carried out. Kinetic simulations for helium plasma are presented and analyzed in Sec.III B 2 and for nitrogen plasma in Sec.III B 3. The plasma conditions are given in their respective sections.

A. pF3D simulations of laser light backscatter and growth of Ion Acoustic waves

The analysis of SBS backscatter from pure gold plasmas[7] in NIF ICF hohlraums for the BigFoot design[40, 41] found that most of the laser power was scattered over the first speckle length ($\sim$ 0.02cm) layer of gold plasma where the plasma flow velocity has very weak gradients. Those simulations used the laser smoothing techniques that are standard at the NIF laser facility, Random Phase Plates (RPP) and polarization smoothing (PS). Reference 7 also simulated SBS from hohlraums where the gold ablated from the hohlraum wall was replaced with a hot Ta_2O_5 plasma. Those simulations

showed the laser intensity threshold for significant SBS was double that of a pure gold plasma because the oxygen ions increase the IAW damping rate more than an order of magnitude (see Fig. 10 of Reference 7). Because of the increased damping the SBS backscatter occurs over a longer length in Ta_2O_5 plasma than in pure gold, approximately four times longer.

Here, we find the same dependence of the SBS on laser intensity for Ta_2O_5 as found in Reference 7 with pF3D simulations of a Ta_2O_5 plasma with $T_e = T_i = 5$keV, $n_e/n_c = 0.1$ and plasma length, $L = 0.072$ cm, that is, four laser speckles long. These simulations, similar to the recent study of filamentation,[42] have a constant density and temperature and no flow. The laser beam enters the plasma at $z = 0$, and the SBS grows from thermal noise.[38] The charge state, Z, of tantalum is taken to be 50. The pF3D simulations assume that the linear damping rates of the IAW are not modified by trapping. Large IAW amplitudes might invalidate that assumption. In RPP smoothed laser beams the SBS light and the associated IAWs grow preferentially in speckles with intensity 2-5 times the average laser intensity. Because the laser intensity varies from speckle to speckle, the intensity of the reflected light and the IAW amplitudes do also.

The SBS reflectivity and the fraction of the plasma area with IAW amplitude greater than 1% of the electron density are shown in Fig.2a as a function of the average laser intensity. The SBS grows from thermal noise to saturation in about 20ps. After saturation the SBS fluctuates in magnitude but the excursions about the average decrease as the number of laser transit times increase. The peak-to-average fluctuation ratio is larger near the threshold. The reflectivities in Fig.2a are a 40ps time average ($\sim$ 16 light transit times) of the saturated SBS. In Fig.2b, the distribution function of the IAW amplitude is shown at $z = 0$, the location of the maximum convective amplification, for six different average laser intensities and smoothing choices.

Below the intensity threshold for SBS without PS, the IAW fluctuation level does not grow in pF3D and remains below 10^{-4} as shown in Fig.2b (red curve). With PS, the intensity threshold increases by 50% as shown by the blue and red curves in Fig. 2a but there is an interesting increase in the IAW amplitudes below the PS threshold, meaning that there is some growth in the more intense speckles (cyan curve). Above the RPP threshold ($\sim 1 \times 10^{15}$W/cm^2), Fig.2b shows a large increase in the fraction of area with large amplitude IAWs (black curve), and this fraction remains large at 1.5×10^{15}W/cm^2 with PS (blue curve). The importance of polarization smoothing (PS) to controlling SBS at the NIF is evident in Fig.2a even if trapping were not a concern. The predicted amplitudes of IAWs are large without PS even when the reflectivity is small, *e.g.* greater than 20% of the laser beam has IAW amplitudes greater than 0.01 when the predicted SBS is $\sim$ 1%. Thus, IAWs with amplitude $\delta n/n_e \sim 1\%$ are of interest to investigate with LOKI Vlasov simulations.

A more thorough study of the IAW amplitudes associated with SBS in spatially smoothed laser beams deserves more attention but is beyond the scope of this paper. Here, our aim is to demonstrate ample reason to concentrate on evaluating the effectiveness of collisions on de-trapping and maintaining the strong IAW Landau damping provided by oxygen in Ta_2O_5 plasma.

B. Kinetic simulations of collisional de-trapping of particles from IAWs

Following the procedure we used previously for single-ion species and collisionless plasma[20], we use an external field in the electron Vlasov equation to drive the waves at the calculated resonant frequency for many wave periods and then turn the drive off to measure the self-consistent frequency and damping rate. The magnitude of the external ponderomotive drive was chosen to drive IAW amplitudes up to $\sim 1\%$ to be relevant to the amplitudes discussed in Sec III A The collisional interactions include self-collisions for each species (electrons and all ions), pitch-angle collisions of the electrons from all ion species, and ion-ion interspecies collisions. All velocities are normalized by the electron thermal velocity, length to the electron Debye length, and frequency, damping, and collision rates to the electron plasma frequency. The spatial average of electron distribution integrates over velocity to one. The spatial average of each ion distribution multiplied by its charge is its atomic fraction of the electron density such that the sum of the total ion charge and electron charge sums to zero. The results for Ta_2O_5 are presented in Sec. III B 1, for helium in Sec. III B 2, and for nitrogen in Sec. III B 3.

1. *Heavy and Light Ion Plasmas:Tantalum-Oxide*

Fig. 3 shows examples of the time dependence of the field amplitude for collisionless and collisional simulations. In the collisionless case, there are noticeable oscillations in the IAW amplitude with a frequency approximately equal to the bounce frequency of the trapped oxygen ions, consistent with previous collisionless simulations of multi-ion-species plasma[33] The ion bounce oscillation frequency of the oxygen ions divided by ω_{pe}, the electron plasma frequency, is $\omega_{bi}/\omega_{pe} = 1.6 \times 10^{-3}$ if $\delta n/n_e = e\phi/T_e = 0.015$. Here, $\delta n/n_e$ is the amplitude of the density perturbation of the IAW divided by the local electron density.

Without collisions, the field initially decays after the drive is turned off but then recovers as the trapped particles return energy to the field. The maximum electrostatic fields for several drive amplitudes with the same collisional rates is also shown in Fig. 3. With collisions, the field damps exponentially over many orders of magnitude, and the rate of decay increases slowly as the particles in the tail of the ion distributions thermalize. With the smaller drives there is no sign of bounce

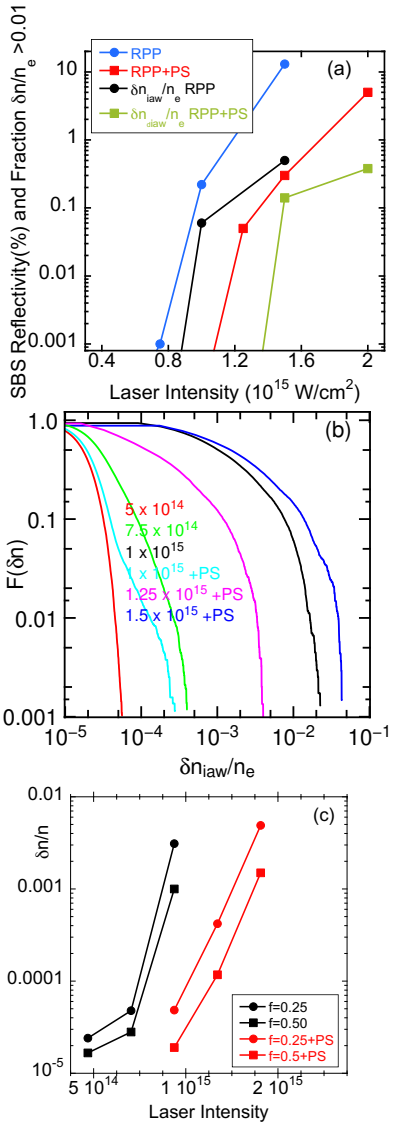

FIG. 2: (a) The SBS reflectivity and the value of the distribution for IAWs with amplitude above 0.01 as a function of the incident average laser intensity for a Ta_2O_5 plasma. (b) The distribution function of the IAW density wave amplitude as a function of the wave amplitude at $z = 0$ for different average laser intensities in W/cm^2 and laser smoothing choices from pF3D simulations. (The minor tick marks are at 0.15, 0.2, and 0.5 of the major marks on the vertical axis and at 0.2 and 0.5 on the horizontal axis.) (c) The density perturbation, $\delta n/n_e$, above which $F(\delta n)$ is 0.25 and 0.50 respectively with and without polarization smoothing. The plasma electron density, the ion and electron temperatures, and plasma length were the same in all cases. Note for a NIF 50° quad at a power of 10TW, the average laser intensity is approximately 1.6×10^{15}W/cm^2

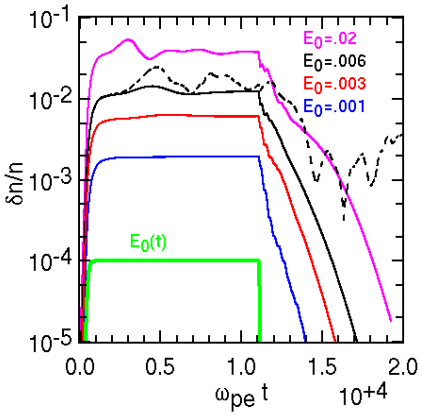

FIG. 3: The maximum amplitude of the IAW as a function of time is shown for external drive fields with maximum values: $E_0 = 0.001, 0.003, 0.006,$ and 0.02. The time dependence of the external drive field, $E_0(t)$, is shown in green. A collisionless example with $E_0 = 0.006$ is shown by the dashed line. (The minor tick marks are at 0.2 and 0.5 of the major marks on the vertical axis.)

oscillations in the field amplitude. The maximum field amplitude is initially set by the linear damping rate as seen by comparing the cases where $E_0 = 0.006$ with and without collisions. (The electric field is normalized to $T_e\lambda_{De}/e$). Only after a bounce oscillation of the trapped oxygen is there a further increase in the field amplitude in the collisionless simulations.

With collisions, a significant effect is that the damping rate is reduced from the initial value of $\gamma_0/\omega_r = 0.21$ to $\gamma/\omega_r = 0.08$ ($\gamma/\omega_{pe} = 0.001$) for $E_0 = 0.006$. The lowest drive has a higher damping rate, $\gamma/\omega_{pe} = 2.6 \times 10^{-3}$ after the drive turns off which is approximately the initial value of the damping rate within the uncertainty of the fit. The damping rate decreases with the wave amplitude as shown in Fig. 4 provided $\delta n/n_e > 1 \times 10^{-4}$ for these parameters. Only if the wave amplitude is at least an order of magnitude smaller than estimated in Eq. (15) or Eq. (16) is the linear Landau damping rate unmodified.

The effect of collisions on the ion distributions is shown in Figs. 5 and 6. Fig. 5a shows the oxygen (O) ion distribution in the collisionless case at a time after the drive is turned off. The ions with $v_x \approx v_{ph}$ are trapped in the

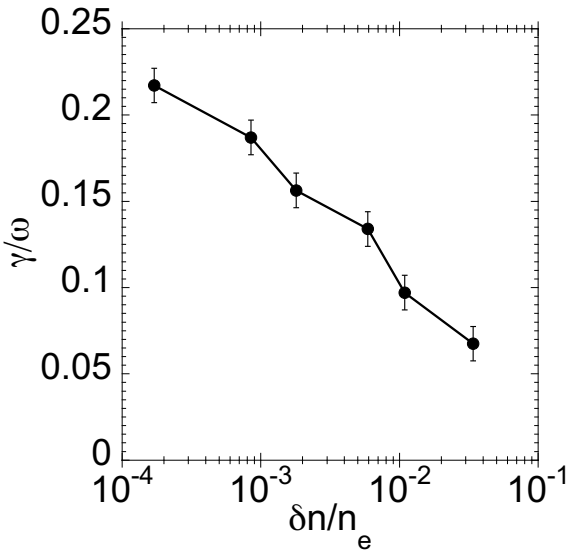

FIG. 4: The Landau damping rate of an IAW including collisions for a Ta_2O_5 plasma as a function of the driven wave amplitude. The analytic value of the damping for the initial plasma parameters is used at $\delta n/n < 10^{-4}$. The error bars are estimated by the variation of the damping rate obtained by measurement over different time intervals after the drive is turned off. The damping rate as a function of amplitude for $x = \delta n/n_e > 10^{-4}$ is approximated by $\gamma/\omega_r = -0.0262 - 0.06667\log_{10}(x)$

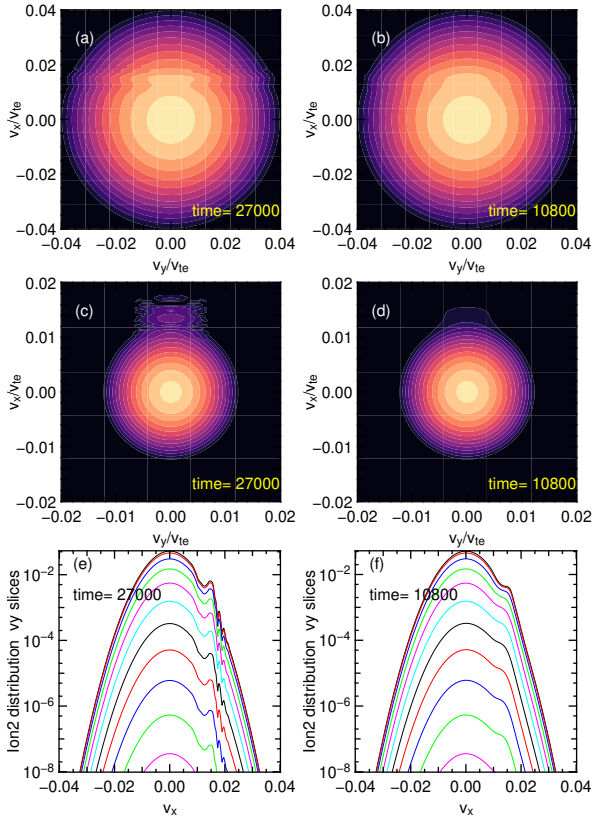

FIG. 5: The ion distributions on a log scale as a function of v_x/v_{te} and v_y/v_{te} for the oxygen ions in a (a) collisionless and (b) collisional simulation and for the tantalum ions in a (c) collisionless and (d) collisional simulation. Figures (e) and (f) show cuts of the oxygen distribution as a function of v_x/v_{te} for equally spaced values of v_y/v_{te} from 0 to 0.02 for the collisionless and collisional simulations shown in panels (a)-(b). (The vertical minor tick marks are at 0.2 and 0.5 of the major interval. The horizontal minor tick marks are at 0.5 in both (e) and (f))

field for all v_y as is true for the (many fewer) tantalum (Ta) ions shown in Fig. 5c. The dominant effect of the scattering of the O ions from the Ta ions is to isotropize the O ions as shown in Fig. 5b. The Ta self-collisions reduce the number and increase the slope of the distribution of trapped Ta ions as shown in Fig. 5d. The 1D plots of the O ion distribution $F_O(v_x, v_y)$ for uniformly distributed values of $0 \leqslant v_y \leqslant 0.02 v_{te}$, shown in Fig. 5e and Fig. 5f in the collisionless and collisional case respectively, quantitatively illustrate the maintenance by collisions of a monotonically decreasing distribution with velocity magnitude. That ensures that O maintains its role in Landau damping IAWs and suppressing the growth of SBS. Fig. 6 isolates the O distribution near $v_x = v_{ph}$ for various drive field amplitudes in a collisional simulation and, in a high drive case, a collisionless simulation. For the lowest drive shown with collisions, the modification of the distribution is slight. Because the wave damping is preserved with collisions, the plasma is continuously heated while the IAW is driven. Over long time scales, heat transport and temperature equilibration between the ions and with the electrons must be considered but cannot be treated with these one-wavelength-long, short-duration simulations.

Fig. 6 is a snapshot that is not necessarily representative of the distribution at other times, especially in the collisionless case. Fig. 7 shows the distribution in the trapping region for a number of times during and after the drive is turned off. During the period when the amplitude is maintained by the external field, the collisionless distribution in the trapped region executes large bounce oscillations with a large bump when the field amplitude is a minimum. The collisional distribution varies little until the external field drive is turned off. Then the distribution (when the drive is off) quickly returns to a Maxwell-Boltzmann form albeit at a higher temperature. The slope of the distribution can be positive or negative at the phase velocity in the collisionless case. It is always negative in the collisional case.

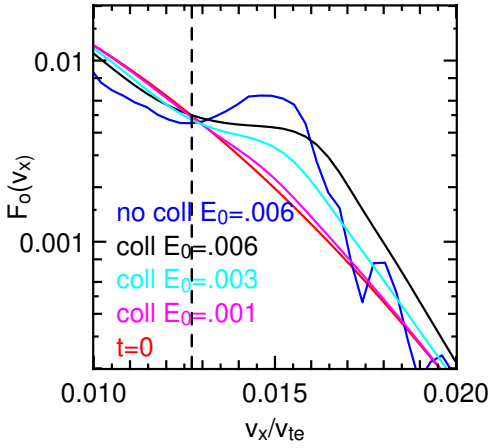

FIG. 6: The oxygen ion distribution at $v_y = 0$ as a function of v_x for a collisionless case with maximum driver field amplitude, $E_0 = .006$, and with collisions for maximum driver field amplitudes, $E_0 = .001, .003, .006$, and for the initial distribution. For weak drive amplitudes, collisions prevent substantial modification near the phase velocity indicated by the vertical dashed line.

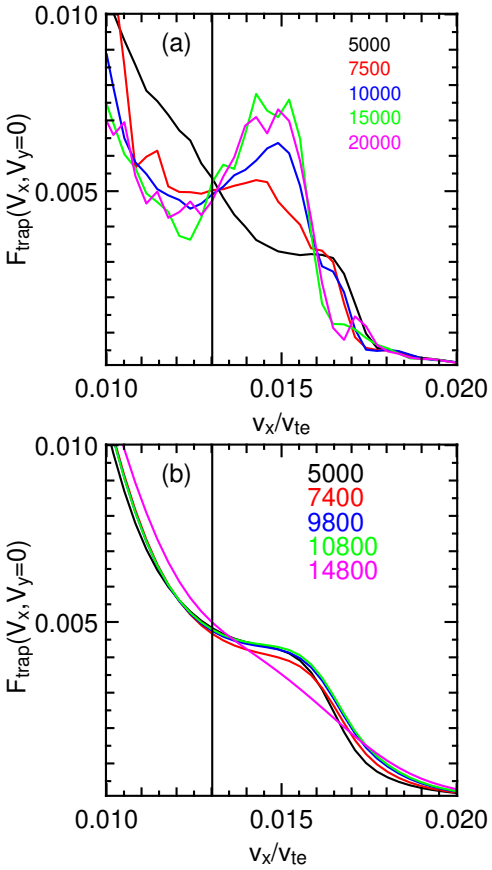

FIG. 7: The oxygen ion distribution averaged over one spatial wavelength along x at $v_y = 0$ as a function of v_x at several different times for (a) a collisionless case and (b) with collisions.

2. *Strongly Damped, One Ion Species Plasma:Helium*

In ICF hohlraums, helium or a mixture of hydrogen and helium fill the hohlraum interior inside the walls and exterior to the capsule to cool the cryogenic DT fuel in the capsule before the laser pulse heats the hohlraum interior. Afterward, that hot plasma serves to impede the expansion of the gold wall into the path of the laser beams. The compression of the helium plasma heats the ions to temperatures comparable to the electron temperature. The electrons are heated by inverse bremsstrahlung and electron heat conduction. The IAW in this plasma is strongly Landau damped because $v_{\rm ph} \sim v_{\rm thi}$. Thus spontaneous SBS is unlikely to grow enough to modify the ion distribution in the helium plasma if the growth occurs only in helium. However, SBS amplified in the gold plasma and propagating backward through the helium coupled with the laser can drive resonately drive IAWs in helium because of Doppler shifts from plasma flows. This process may produce a large enough ponderomotive drive to trap helium ions and lower the damping rate. The ponderomotive drive of crossing laser beams could also. In this section, we study the effect of collisions on maintaining the IAW damping in the presence of strong ponderomotive drive. As discussed in Sec. II, the frequency and damping of an IAW in fully ionized helium with $n_e = 0.05 n_c$, $T_e = 2T_i = 4$ keV, Z=2, and A=4, are $\omega/\omega_{pe} = (1.60 - 0.312i) \times 10^{-2}$, that is, $\gamma/\omega_r = 0.195$.

In the collisionless case, the fields maintain their amplitude after the drive is turned off. The oscillations in the wave amplitude are approximately the period of a trapped helium ions. For the stronger drive the collisions in this low Z plasma are not sufficient to fully eliminate bounce oscillations in the field amplitude that are similar to those for the collisionless case. However, once the ponderomotive drive is turned off, the wave damps quickly at a reduced Landau rate. A lower amplitude wave damps more quickly. This behavior, shown in Fig. 8, is expected and very similar to the wave evolution for a Ta_2O_5 plasma shown in Fig.3.

3. *Weakly Damped Ion Acoustic Waves in Cold Single-Ion Species Plasmas:Nitrogen*

Motivated by experiments with 100 Joule scale lasers, previous studies of trapped ions and electrons in IAWs were done for low temperature, low Z plasmas ($T_e =$ 600eV, $T_i < 150$eV, $n_e/n_c = 0.05$, $Z = 7$, $A = 14$). [32] In this case, n_c is the critical density for 0.527μm laser light. The IAWs were weakly damped and driven by the large ponderomotive forces with high SBS backscatter (~ 50 %) in localized f/6, 0.527μm intense laser speckles where the laser intensity $I_L \lesssim 2.5 \times 10^{15}$W/cm^2.

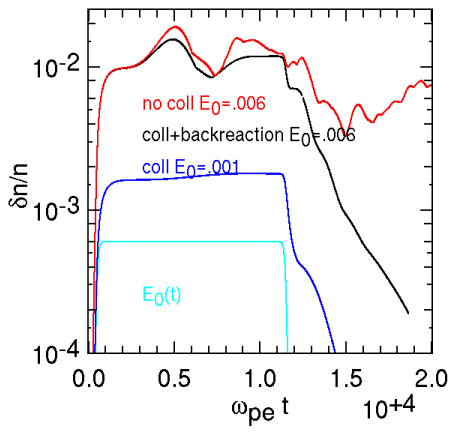

FIG. 8: The maximum amplitude of the IAW as a function of time is shown for two drive amplitudes in a helium plasma. The time dependence of the drive field, $E_0(t)$, is shown in cyan. The maximum value of the drive field is given for each case in the legend. The minor interval tick marks on the vertical axis are at 0.15,0.2,0.3,0.4,0.5 and 0.8 of the major interval; The 10 horizontal minor tick marks are equally spaced between the major intervals.

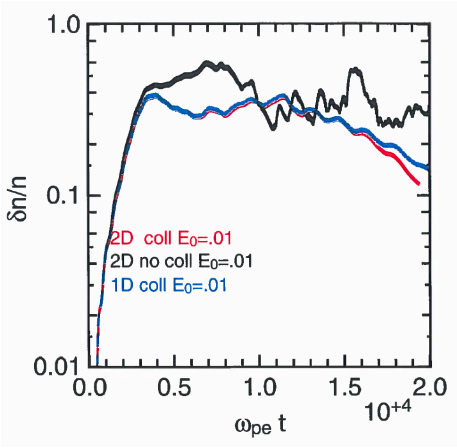

FIG. 9: The maximum amplitude of the IAW density perturbation in a cold Nitrogen plasma is shown as a function of time for a drive field amplitude, $E_0 = 0.01$ for 1D and 2D simulations with and without collisions. The drive field time dependence is the same as shown in Fig. 3. There is little sensitivity to number of dimensions. The minor interval tick marks on the vertical axis are at 0.15,0.2,0.3,0.4,0.5 and 0.8 of the major interval; The 10 horizontal minor tick marks are equally spaced between the major intervals.

The oscillatory velocity in the laser electric field E_L is $V_0 = eE_L/(m_e\omega_L)$ where ω_L is the laser frequency. In this case, $V_0/v_{\rm the} \sim 1$ in contrast to NIF where $V_0/v_{\rm the} \lesssim 0.1$. Because of the relatively low ion and electron temperatures, collision rates are significant, and simulations with collisions significantly differ from collisionless ones. The collisional mean free path for thermal electrons is, $\lambda_{ei} = 5.3 \times 10^{-4}$ cm. For thermal ions, the self-collisional ion-ion mean free path is, $\lambda_{ii} = 3.5 \times 10^{-6}$ cm. The detrapping conditions for a single ion plasma were given in the Appendix of Ref.20. In this case transverse diffusion for electrons and ions leads to approximately the same limit, namely $\delta n_e/n_e < 0.05$

However, the IAW remains weakly damped and, as shown in Sec. IV, does filament in both the collisional and collisionless simulations. Because the wave is weakly damped, with or without collisions, the wave amplitude, shown in Fig. 9 is more than an order of magnitude greater than the drive field, unlike the strongly damped cases shown in the previous sections. After the external field turns off at $\omega_{pe}t = 1 \times 10^4$, the wave damps slowly in the presence of collisions. The damping rate is nearly the same for one and two dimensions.

IV. SELF FOCUSING OF LARGE AMPLITUDE LOCALIZED ION ACOUSTIC WAVES

In the SBS backscatter of laser light, the IAWs grow in transversely localized intense laser speckles of transverse size, $l_s \approx f\lambda_0$ where f is the f-number of the focusing optic and λ_0 is the laser wavelength. The IAW driven by SBS backscatter has wavelength, $\lambda_{iaw} \approx \lambda_0/2$, and the transverse width is determined by the beat ponderomotive force of the overlapping incident laser and backscattered light wave. A reasonable estimate is to take that width to be the laser speckle width, l_s. In this section, we consider LOKI simulations in two spatial dimensions to study the self-focusing of driven IAWs for plasma parameters of interest to ignition hohlraums and to plasmas used for basic laser-plasma interactions, specifically SBS. The parameters of the LOKI simulations are given in the subsections examining each case. Based on the work done on the self-focusing of electron plasma waves[29, 43–46], one expects that IAWs will also self focus if the frequency shift is negative (because the shift from the ions exceeds the shift from electrons[20, 33, 47]), the shift varies transversely across the speckle with the largest magnitude shift on axis, and the IAW amplitude is large enough. In the Appendix, Sec VI, IAW and EPW self-focusing is explained by an analogy with the well-known ponderomotive self-focusing of a light wave.

For small perturbations, self-focusing can be represented with a nonlinear Schrödinger equation for the wave amplitude $a(x,y,t) = a_k(x,y,t)\exp(-i\omega_k t + ik_x x) + c.c$,

$$\left(\frac{\partial}{\partial t} + v_{gx}\frac{\partial}{\partial x} + \nu - iD_{yy}\frac{\partial^2}{\partial y^2} - i\Delta\omega\right) a_k = 0, \quad (18)$$

where ω_k and k_x are taken to satisfy the dispersion relation in the unperturbed plasma. For example, the light

wave dispersion is $\omega_0 = \sqrt{c^2 k_{x,0}^2 + \omega_{pe,0}^2}$. The coefficients are obtained from the wave dispersion relations as $v_{gx} = \partial\omega_k/\partial k_x$, $D_{yy} = \partial^2\omega_k/\partial k_y^2/2$, and $\Delta\omega$ is the difference of the local amplitude dependent frequency from ω_k. The dispersion relations in the fluid approximation for the light ϵ^T, the EPW ϵ_L, and the IAW ϵ_a are given respectively by

$$\epsilon^T(\vec{k},\omega) = c^2k^2 + \omega_{pe}^2 - \omega_k^2 \tag{19}$$

$$\epsilon_L(\vec{k},\omega) = 1 - \frac{\omega_{pe}^2}{\omega^2 - 3k^2v_{te}^2} \tag{20}$$

$$\epsilon_a(\vec{k},\omega) = 1 + \frac{1}{k^2\lambda_{De}^2} - \frac{\omega_{pi}^2}{\omega^2 - 3k^2v_{ti}^2} \tag{21}$$

The group velocity, $v_{gx} = c\sqrt{1-\omega_{pe}^2/\omega_k^2}$ for a light wave, $v_{gx} = 3kv_{te}^2/\omega_k$ for an EPW, and $v_{gx} = k(C_s^2 + 3v_{ti}^2)/\omega_k$ where $C_s = \lambda_{De}\omega_{pi}$ for a single-ion species IAW in the limit $k\lambda_{De} \ll 1$, The diffractive term, $D_{yy} = c^2/(2\omega_k)$ for a light wave, $D_{yy} = 3v_{te}^2/(2\omega_k)$ for an EPW, and $D_{yy} = (C_s^2 + 3v_{ti}^2)/(2\omega_k)$ for a single-ion species IAW. For multiple-ion species in hot plasma as we simulate in this work, these fluid approximations are not accurate and numerical solutions to the plasma dispersion relations would be required for Eq. (18).

For a light wave and an electron plasma wave, the frequency is lowered as the wave amplitude is increased. For an IAW the frequency is increased by the trapped electrons and decreased by the trapped ions.[20, 47] Thus, the IAW nonlinear focusing or defocusing depends on the magnitudes of the frequency shifts from each species.

In an electron plasma wave, loss of trapped electrons from 'sideloss'[48] at the rate τ_{se}^{-1}, where $\tau_{se} = l_s/v_{te}$, is a limiting factor on the wave amplitude and reduces the variation of the amplitude transversely. That also affects the trapped electrons in an ion acoustic wave but is not significant for trapped ions because the sideloss rate from the ion thermal velocity, $\tau_{si}^{-1} \ll \tau_{se}^{-1}$, where $\tau_{si} = l_s/v_{ti} \gg \tau_{se}$. In general, collisions are the limiting factor for the frequency shift variation from the trapped ions, especially for high-mass, high-Z ions considered in the next section.

Heavy and Light Ion Plasmas

Tantalum-Oxide

The plasma parameters for the LOKI simulations in this section are the same as in Sec. II, stationary ionized tantalum-oxide with (Z=50,8), (A=181,16), and with $n_e = 0.05n_c$ and $T_e = T_i = 5$ keV. Using a external driving ponderomotive field of magnitude, $E_0 = 0.006$ with frequency and wavenumber chosen to drive an IAW at resonance for these plasma parameters and as used in Fig. 3 and width l_s with $f = 8$, we show in Fig. 10 that the sideloss plays a minor role in limiting the amplitude

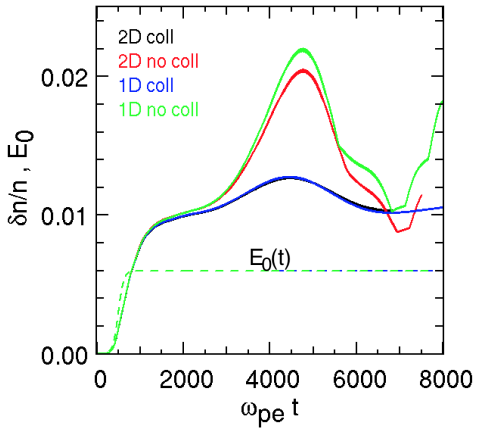

FIG. 10: Comparison of the time dependence of the maximum IAW amplitude in Ta_2O_5 plasma for the same external driving field for 1D and 2D without collisions and 1D and 2D with collisions. With collisions, there is very little difference between 1D and 2D. The maximum of the driving electric field, E_0, shown by the overlapping dash lines is the same for all cases.

of the IAW as the maximum wave amplitude in a 1D simulation without sideloss and in a 2D simulation with sideloss have nearly the same behavior. There is also no enhancement of the wave amplitude from self focusing.

If the frequency shift is dominated by the lighter ions, a reasonable estimate of the transverse variation of frequency shift in a localized IAW wave can be made from the variation with amplitude of the frequency shift from the 1D simulations. With the drive off, there is a sizeable negative shift as a function of the amplitude but the wave decays so quickly that the self focusing process is irrelevant. While the drive is on, the frequency is determined by the drive frequency and is independent of amplitude.

Neglecting collisions on all species, we find that IAWs do form mildly curved wavefronts and may break up transversely as shown in Fig. 11. In the collisional case, the maximum amplitude is reduced almost twofold and, although Fig. 12 shows some tendency to curved wavefronts, the wave does not break up transversely.

Weakly Damped Ion Acoustic Waves in Cold Single-Ion Species Plasmas:Nitrogen

LOKI simulations of driven IAW in two spatial dimensions are considered for the same parameters as in Sec. III B 3, namely $T_e = 600$eV, $T_i < 150$eV, $n_e/n_c = 0.05$, $Z = 7$, $A = 14$ where, in this case, n_c is the critical density of 527nm light. The FWHM of the driving field is taken as the laser speckle width, $l_s = f\lambda_0$, as is done for Ta_2O_5, where in this case $f = 6$ and $\lambda_0 = 527$nm. In Figs. 13 and 14, lengths are in units of the electron Debye length, $\lambda_{De} = 1.3 \times 10^{-6}$cm and

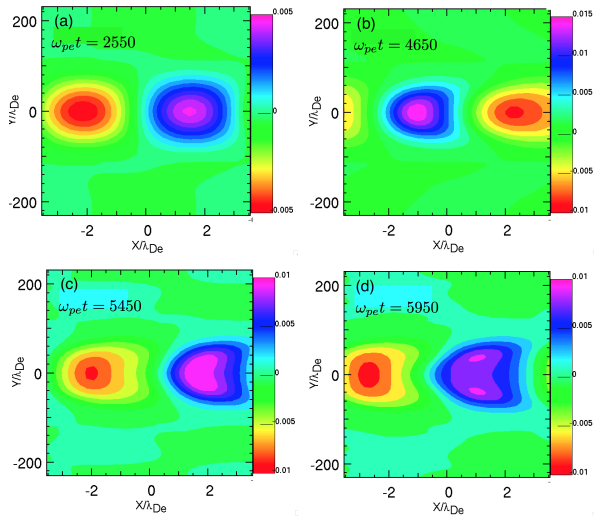

FIG. 11: The IAW electric field from a collisionless LOKI simulation propagating to the right in a one wavelength long periodic Ta_2O_5 plasma and localized in the driving ponderomotive force at a sequence of times: (a) $\omega_{pe}t = 2550$ before the 'inflation', (b) $\omega_{pe}t = 4650$ at the peak amplitude, (c) $\omega_{pe}t = 5450$ when the wavefronts are bowed, and (d) $\omega_{pe}t = 5950$ at breakup.

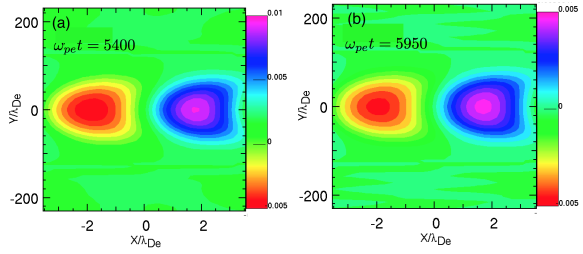

FIG. 12: The IAW electric field from a collisional LOKI simulation propagating to the right in a one wavelength long periodic Ta_2O_5 plasma and localized in the driving ponderomotive force at times (a) $\omega_{pe}t = 5400$ and (b) $\omega_{pe}t = 5950$. In the collisionless case, the wavefronts are bowed when $\omega_{pe}t = 5400$ and at breakup when $\omega_{pe}t = 5950$.

$l_s/\lambda_{De} = 246$. The self-focusing of the IAW in this case with $E_x(\max) \approx 0.1$ is similar with and without collisions. Note, $e\phi/T_e = \delta n_e/n_e \approx E_x/(k\lambda_{De}) = 0.3$ which greatly exceeds the detrapping estimate $\delta n_e/n_e < 0.05$. For that reason, we show the collisional results, the more physically relevant case. For a drive field ten times smaller and the same pulse length, the IAW amplitude is 2.5 times smaller but is still growing when the drive is turned off. The higher drive case saturates earlier and nonlinearly. In the lower drive case, the wavefronts remain concave during and after the drive field is turned off. Then, since the electron induced frequency shift exceeds the ion shift, no self-focusing occurs which is qualitatively different from the results in Ref. 32.

In our study of EPW self-focusing[46], $W_E(y,t) = \int dx E^2(x,y,t)$ clearly demonstrated the focusing of the wave. The field energy density, $E^2(x,y,t)$, is positive but includes spatial variation along the propagation direction that is not useful to illustrate the transverse variation of the wave envelope. $W_E(y,t)$, the spatial average of the field energy density along the propagation direction isolates the transverse variation and the time at which self-focusing begins. In Fig. 13a, $W_E(y,t)$ shows a reduction in the transverse envelope with time especially after the external field is turned off. This quantity, applied to the Ta_2O_5 simulations, showed no reduction in the transverse envelope. The spatial averaging in $W_E(y,t)$ hides some interesting details that the snapshots in Fig.13b-d show: the steepening of the wave from harmonic generation and wavefront curvature from positive frequency shifts in Fig. 13b, followed at later time by wavefront curvature from negative frequency shifts near the y-axis and the positive curvature at larger radius from positive frequency shifts in Fig.13c, and the breakup transversely after the drive field is turned off in Fig.13d.

In this evolution, the IAW does not filament while it is driven because the curvature of the wavefronts are dominated by the electrons. Afterward, the trapped electrons are depleted by the electron ion collisions and side-loss faster than the trapped ions are. That evolution is shown in Fig.14a-d. Fig.14a shows that, while the external field is applied, the trapped electrons are localized transversely in the wave. Fig.14b shows that, while the external field is applied, the trapped ions are more localized transversely in the wave than the electrons are at the same time. Fig.14c shows that, after the external field is off, heated electrons broaden the distribution along V_x and lower the number at low velocity and that the trapped electrons leave the heated region. Fig.14d shows the trapped ions are scattered in angle and are trapped over a larger region transversely but remain in the heated region after the external field is off. Thus, they cause a negative frequency shift in the IAW except at the edge where an excess of electrons remain. Examining Fig. 13c and d, one can see the reversal of the wavefront curvature where the frequency shift changes from negative to positive. One of the examples in Fig. 10 in Ref. 32 shows a similar behavior.

V. HEATING AND ENERGY CONSERVATION

The energy transferred from the external field to the plasma kinetic energy and to the fields for single-ion and two-ion species plasmas is discussed in this section for collisionless and collisional 1D+2V simulations. Helium and tantalum-oxide are considered. In both cases, the light ions absorb most of the acoustic wave energy driven by the ponderomotive drive at the IAW resonant frequency simply because the ion damping is much larger than the

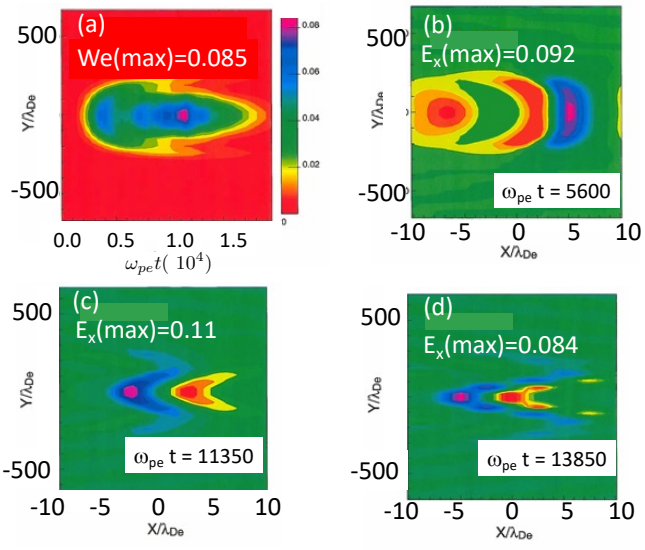

FIG. 13: Single-ion Nitrogen plasma (a) The variation of $W_E(y,t)$ with time the external field is turned off at $\omega_{pe}t = 10^4$. (b)-(d)The spatial variation of $E(x,y)$ at 3 times. (b) $E(x,y)$ at $\omega_{pe}t = 5.6\times10^3$, (c) $E(x,y)$ at $\omega_{pe}t = 1.135\times10^4$, (d) $E(x,y)$ at $\omega_{pe}t = 1.385\times10^4$

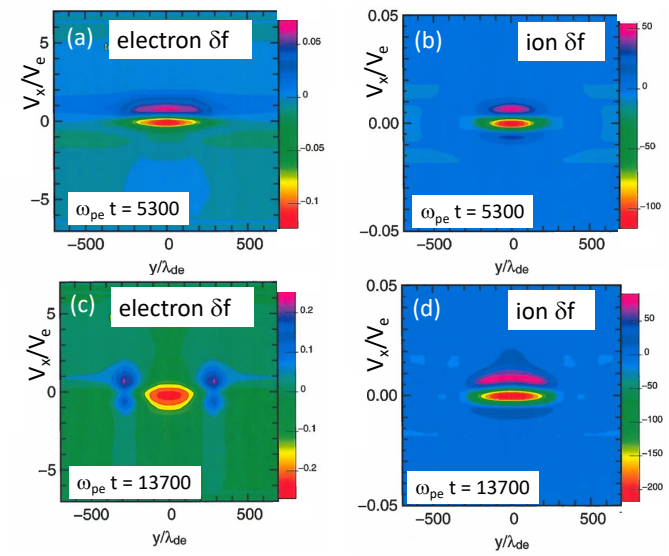

FIG. 14: Single-ion Nitrogen plasma. The difference of the perturbed electron and ion distributions from the initial Maxwell-Boltzmann, $\delta f = \int dv_y dx(f(x,y,v_x,v_y,t) - f(x,y,v_x,v_y,0))$, at $\omega_{pe}t = 5300$ while the external field is on and at $\omega_{pe}t = 13700$ after the field is turned off.

electron damping.

In Fig. 15a,b, the energy in the electrostatic field and the kinetic energy in each species is shown as a function of time during the time the external field is on and after for the collisionless simulations. The components of the total energy continue to evolve after the external field is zero but the total plasma energy equals the added energy within 0.7% for the helium plasma and within 0.4% for the two-ion species plasma at all times. The total energy is constant after the external field is zero. Because of particle trapping the plasma returns energy to the driver during the bounce oscillations.

In Fig. 15c,d, the energy in the electrostatic field and the kinetic energy in each species is shown as a function of time during the time the external field is on and after for the collisional simulations. The components of the total energy continue to evolve after the external field is zero. The total plasma energy equals the added energy within 0.1% for the helium plasma and within 3% for the two-ion species plasma at all times. The total energy is constant after the external field is zero. Because ion-ion collisions are weak for the helium plasma, weak particle trapping persists and plasma energy does not monotonically increase while the external field is on. Strong interspecies collisions maintain Landau damping in the Ta_2O_5 plasma so the total energy monotonically increases while the drive is on. Once the drive is zero, the IAW is rapidly damped, and the kinetic energy of all three plasma species increase at first. Subsequently, the oxygen slows down on the tantalum and loses energy (not visible on the log scale in the figure) as the tantalum energy increases. Interspecies collisions of electrons with ions is treated in the pitch-angle approximation in these simulations. That approximation neglects the direct energy transfer between ions and electrons. Thus the ions are not heated the small amount by the electrons that they are in reality.

The electron kinetic energy increases for a short time just as the ponderomotive drive turns off, particularly noticeable for the helium plasma. Not visible on this log scale plot is a corresponding increase in the total energy and the energy absorbed from the external drive field. The subsequent decrease in the electron kinetic energy is taken up by the ions such that the energy absorbed and the increase in the total energy remain in balance. The Ta_2O_5 plasma has more complicated dynamics overall but the sudden but temporary increase in the electron kinetic energy is similar. In this case, though, the heavy ions pick up kinetic energy some of which comes from the oxygen kinetic energy (not visible in this log scale plot)

VI. CONCLUSION

We have explored the effect of collisions, both self-collisions and interspecies collisions on the damping of large amplitude IAW waves. Indirect-drive ICF plasmas in hohlraums are prone to large SBS when the power and pulse lengths exceed thresholds, especially in the underdense high-Z gold or uranium plasma ablated from the interior of the hohlraum walls. Proposed solutions that re-

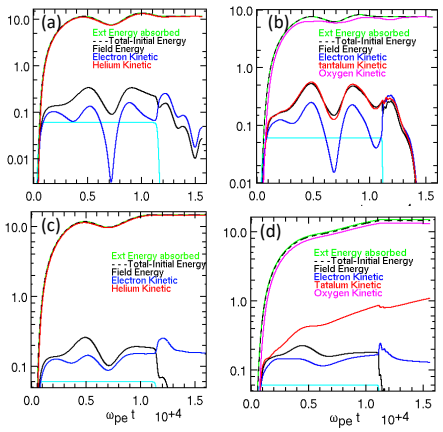

FIG. 15: The increase in the total, field, electron kinetic, and ion kinetic energy for a one-ion and two-ion species plasmas is shown along with the external energy added. The green line is the running total energy absorbed and the dashed line is the total energy minus the initial energy. The components of the total energy are identified by the legend in the figure. (a) a collisionless simulation for one ion species, helium; (b) a collisionless simulation for two ion species, Ta_2O_5; (c) a collisional simulation for one ion species, helium; (d) a collisional simulation for two ion species, Ta_2O_5 In (a)and(b) the minor interval tick marks on the vertical axis are at 0.15,0.2, and 0.5 of the major interval. In (a)and(b) they are at 0.15,0.2,0.3,0.4,0.5 and 0.8 of the major interval; The 10 horizontal minor tick marks are equally spaced between the major intervals.

duced SBS are mixtures of low-Z and high-Z ions such as Ta_2O_5 or AuB that significantly increase the IAW damping rate because the thermal velocity $v_{\rm thi}$ of Oxygen(O) or Boron(B) is comparable to the IAW phase velocity, $v_{\rm ph}$. The linear effect of increased damping from collisions is insignificant in these hot, low-density plasmas. The maintenance of ion Landau damping by collisional de-trapping of O or B by scattering from the high-Z Ta or Au ions is the important effect we have studied. Simulations without collisions show trapping in the large amplitude IAW eliminates the ion Landau damping after a few ion bounce periods. Thus, 'kinetic inflation' would ensue, eliminate the oxygen or boron ion Landau damping after a short period, and simulations would predict large SBS.

Using the criteria, $\omega_{bj}\tau_c < 2\pi$ where τ_c is the relevant collision time, we predict in Sec II the IAW amplitude below which trapping will be mitigated for multiple ion species and single ion species plasmas. The simulations in Sec III quantify the effect for Ta_2O_5 and He plasma for particular choices of plasma parameters that are typical of hohraums at the NIF. There are three wave amplitude regimes. In the lowest range, the collisions maintain the linear ion Landau damping. In the mid-range, the ion Landau rate is reduced by an amount inversely proportional to the wave amplitude as shown in Fig.4. For very large wave amplitudes, collisions have a minor effect while the ponderomotive drive is on.

For helium plasma with NIF-like plasma conditions, the maximum IAW amplitude versus time shown in Fig.8 is very similar to Ta_2O_5 shown in Fig.3 for the same ponderomotive drive amplitude.

Also simulated was the effect on a nitrogen plasma that was the subject of an SBS experiment with a $\sim$ 100Joule laser. In this case, 1D and 2D simulations show the ion and electron Landau dampings are very weak with or without collisions. Without collisions the damping is nearly zero. In Sec IV, 2D simulations to study the self-focusing of transversely localized IAWs were done for Ta_2O_5 and nitrogen plasmas, the latter with plasma parameters taken from Reference 32. In both cases, results were shown with collisions included. The Ta_2O_5 simulations showed no filamentation of the wave during or after the drive was turned off. The behavior was much more interesting for the nitrogen plasma where the IAW self-focused and subsequently filamented strongly. While the drive was on, the wave fronts were dominated by a positive frequency shift and did not self-focus. Afterward, the sideloss of the trapped electrons allowed self-focusing and filamentation.

The dynamics for an SBS simulation might differ if the IAW frequency was determined locally by properties of the electron and ion distributions including the trapped particles rather than by the ponderomotive drive while it is on. However, if the IAW filamentation in SBS occurs after the interaction is saturated due to detuning, then the filamentation may have little to do with SBS saturation.

Sec V examines energy conservation and partition among the plasma species for collisionless and collisional simulations. While the external ponderomotive drive field is applied, the light ions provide most of the damping and absorb most of the energy. In the collisionless simulations, the damping reverses sign from absorbing to emitting during the bounce period of the light oxygen ion. Thus the total kinetic and IAW field energy does not monotonically increase. Collisional simulations with the same external drive field have almost monotonic increase in plasma energy for the He plasma but a strictly monotonic increase for the Ta_2O_5 plasma. In the latter case, the IAW field energy decays rapidly once the drive is off, the electron kinetic energy decreases to a constant. and the heavy tantalum ions gain energy as they slow down lighter oxygen ions. In all cases, the energy absorbed (computed as the time integral of $\vec{E_0}\cdot\vec{J}$ where $\vec{J}$ is the electron current) is accounted for by the IAW and plasma kinetic energy increase.

Our work illustrates the significant impact collisions make on basic nonlinear wave-particle interactions. Here, only the simplest effect has been examined. Studies of plasma wave nonlinearities and instabilities, including our own, have often treated the plasmas as collision-

less. The results presented here motivate revisiting this work in the presence of collisions, as applying collisionless results to collisional plasmas may lead to qualitatively incorrect expectations or interpretations of SBS behavior. A number of effects that are thought to limit the growth of stimulated Brillouin or Raman scattering, *e.g.* the Trapped Particle Instability.[27] and detuning from trapped particle frequency shifts[49–54] that neglected collisional effects should be simulated in the presence of the appropriate collisional effects. The presence of strong collisions may also allow simpler and more efficient modeling of plasma heating and creation of energetic electrons or ions by justifying the use of quasi-linear diffusion operators on the distribution function.[55]

ACKNOWLEDGMENTS

The authors greatly appreciate the technical reports with details on numerical implementation of Landau collision operators written by Stephan Brunner and generously shared with us. Also, R. L. Berger greatly appreciates the suggestions and insight provided by Bruce I. Cohen. He is greatly indebted to Andrea Kritcher for guidance in the discussion of the recent advances in yield and of the evolution in capsule and hohlraum design. This work was performed under the auspices of the U.S. Department of Energy by Lawrence Livermore National Laboratory under Contract DE-AC52-07NA27344. This document was prepared as an account of work sponsored by an agency of the United States government. Neither the United States government nor Lawrence Livermore National Security, LLC, nor any of their employees makes any warranty, expressed or implied, or assumes any legal liability or responsibility for the accuracy, completeness, or usefulness of any information, apparatus, product, or process disclosed, or represents that its use would not infringe privately owned rights. Reference herein to any specific commercial product, process, or service by trade name, trademark, manufacturer, or otherwise does not necessarily constitute or imply its endorsement, recommendation, or favoring by the United States government or Lawrence Livermore National Security, LLC. The views and opinions of authors expressed herein do not necessarily state or reflect those of the United States government or Lawrence Livermore National Security, LLC, and shall not be used for advertising or product endorsement purposes. The data that support the findings of this study are available from the corresponding author upon reasonable request.

APPENDIX:LIGHT SELF FOCUSING

This self focusing of plasma waves can be understood through an analogy with the familiar ponderomotive self-focusing of a light wave in a plasma. In that process, the light pressure digs a trough whose depth is larger where the intensity is larger and modifies the index of refraction, $\tilde{n}$ such that $\tilde{n}$ is larger where the intensity is larger. Thus the light refracts into lower densities to increase the intensity further. [56] Consider the wave equation for a light wave for the vector potential $\vec{A}$ in a plasma,

$$\left(-\nabla^2 + \frac{\partial^2}{c^2\partial t^2} + \frac{\omega_{pe}^2}{c^2}\right)\vec{A} = 0 \tag{22}$$

Introduce the eikonal aproximation, $\beta(x,y,t)$ and $\vec{A} = \vec{a_k}(x,y,t)\exp i\beta + c.c.$ and find

$$\nabla^2\vec{A} = \exp i\beta\left(2i\frac{\partial\beta}{\partial x}\frac{\partial a_k}{\partial x} - [\frac{\partial\beta}{\partial x}]^2 a_k + (x\rightarrow y)\right) \tag{23}$$

$$\frac{\partial^2\vec{A}}{\partial t^2} = \exp i\beta\left(2i\frac{\partial\beta}{\partial t}\frac{\partial a_k}{\partial t} - [\frac{\partial\beta}{\partial t}]^2 a_k\right) \tag{24}$$

where we have neglected the 2nd derivatives of the phase and wave amplitude, β and a_k, respectively. We introduce the standard definitions, $\omega = -\partial\beta/\partial t$ and $\vec{k} = \nabla\beta$ and find

$$-2i\left(\frac{\partial}{\partial t} + \frac{c^2\vec{k}}{\omega}\cdot\nabla\right)a_k + \omega\left(\frac{c^2k^2}{\omega^2} - 1 + \frac{\omega_{pe}^2}{\omega^2}\right)a_k = 0$$

Where the light wave amplitude has a negligible effect on the plasma density, the frequency is ω_0 and then $\omega = \omega_0 + \Delta\omega(I)$. The surfaces of constant phase β will be either concave or convex if the frequency shift, $\Delta\omega(I)$, is positive or negative respectively. Light waves will diverge for a concave phase surface and focus for a convex phase surface as indicated schematically in Fig. 16.

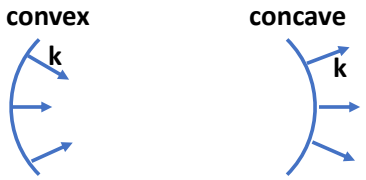

FIG. 16: The surfaces of constant phase for convex and concave lenses. A convex lens causes the light to focus whereas the concave lens causes the light to defocus.

[1] H. AbuShawareb, R. Acree, P. Adams, J. Adams, B. Addis, R. Aden, P. Adrian, B. B. Afeyan, M. Aggleton, L. Aghaian, A. Aguirre, D. Aikens, J. Akre, F. Albert, M. Albrecht, B. J. Albright, J. Albritton, J. Alcala, C. Alday, D. A. Alessi, N. Alexander, J. Alfonso, N. Alfonso, E. Alger, S. J. Ali, Z. A. Ali, W. E. Alley, P. Amala, P. A. Amendt, P. Amick, S. Ammula, C. Amorin, D. J. Ampleford, R. W. Anderson, T. Anklam, N. Antipa, B. Appelbe, C. Aracne-Ruddle, E. Araya, M. Arend, P. Arnold, T. Arnold, J. Asay, L. J. Atherton, D. Atkinson, R. Atkinson, J. M. Auerbach, B. Austin, L. Auyang, A. S. Awwal, J. Ayers, S. Ayers, T. Ayers, S. Azevedo, B. Bachmann, C. A. Back, J. Bae, D. S. Bailey, J. Bailey, T. Baisden, K. L. Baker, H. Baldis, D. Barber, M. Barberis, D. Barker, A. Barnes, C. W. Barnes, M. A. Barrios, C. Barty, I. Bass, S. H. Batha, S. H. Baxamusa, G. Bazan, J. K. Beagle, R. Beale, B. R. Beck, J. B. Beck, M. Bedzyk, R. G. Beeler, R. G. Beeler, W. Behrendt, L. Belk, P. Bell, M. Belyaev, J. F. Benage, G. Bennett, L. R. Benedetti, L. X. Benedict, R. Berger, T. Bernat, L. A. Bernstein, B. Berry, L. Bertolini, G. Besenbruch, J. Betcher, R. Bettenhausen, R. Betti, B. Bezzerides, S. D. Bhandarkar, R. Bickel, J. Biener, T. Biesiada, K. Bigelow, J. Bigelow-Granillo, V. Bigman, R. M. Bionta, N. W. Birge, M. Bitter, A. C. Black, R. Bleile, D. L. Bleuel, E. Bliss, E. Bliss, B. Blue, T. Boehly, K. Boehm, C. D. Boley, R. Bonanno, E. J. Bond, T. Bond, M. J. Bonino, M. Borden, J.-L. Bourgade, J. Bousquet, J. Bowers, M. Bowers, R. Boyd, A. Bozek, D. K. Bradley, K. S. Bradley, P. A. Bradley, L. Bradley, L. Brannon, P. S. Brantley, D. Braun, T. Braun, K. Brienza-Larsen, T. M. Briggs, J. Britten, E. D. Brooks, D. Browning, M. W. Bruhn, T. A. Brunner, H. Bruns, G. Brunton, B. Bryant, T. Buczek, J. Bude, L. Buitano, S. Burkhart, J. Burmark, A. Burnham, R. Burr, L. E. Busby, B. Butlin, R. Cabeltis, M. Cable, W. H. Cabot, B. Cagadas, J. Caggiano, R. Cahayag, S. E. Caldwell, S. Calkins, D. A. Callahan, J. Calleja-Aguirre, L. Camara, D. Camp, E. M. Campbell, J. H. Campbell, B. Carey, R. Carey, K. Carlisle, L. Carlson, L. Carman, J. Carmichael, A. Carpenter, C. Carr, J. A. Carrera, D. Casavant, A. Casey, D. T. Casey, A. Castillo, E. Castillo, J. I. Castor, C. Castro, W. Caughey, R. Cavitt, J. Celeste, P. M. Celliers, C. Cerjan, G. Chandler, B. Chang, C. Chang, J. Chang, L. Chang, R. Chapman, T. Chapman, L. Chase, H. Chen, H. Chen, K. Chen, L.-Y. Chen, B. Cheng, J. Chittenden, C. Choate, J. Chou, R. E. Chrien, M. Chrisp, K. Christensen, M. Christensen, A. R. Christopherson, M. Chung, J. A. Church, A. Clark, D. S. Clark, K. Clark, R. Clark, L. Claus, B. Cline, J. A. Cline, J. A. Cobble, K. Cochrane, B. Cohen, S. Cohen, M. R. Collette, G. Collins, L. A. Collins, T. J. B. Collins, A. Conder, B. Conrad, M. Conyers, A. W. Cook, D. Cook, R. Cook, J. C. Cooley, G. Cooper, T. Cope, S. R. Copeland, F. Coppari, J. Cortez, J. Cox, D. H. Crandall, J. Crane, R. S. Craxton, M. Cray, A. Crilly, J. W. Crippen, D. Cross, M. Cuneo, G. Cuotts, C. E. Czajka, D. Czechowicz, T. Daly, P. Danforth, R. Darbee, B. Darlington, P. Datte, L. Dauffy, G. Davalos, S. Davidovits, P. Davis, J. Davis, S. Dawson, R. D. Day, T. H. Day, M. Dayton, C. Deck, C. Decker, C. Deeney, K. A. DeFriend, G. Deis, N. D. Delamater, J. A. Delettrez, R. Demaret, S. Demos, S. M. Dempsey, R. Desjardin, T. Desjardins, M. P. Desjarlais, E. L. Dewald, J. DeYoreo, S. Diaz, G. Dimonte, T. R. Dittrich, L. Divol, S. N. Dixit, J. Dixon, E. S. Dodd, D. Dolan, A. Donovan, M. Donovan, T. Döppner, C. Dorrer, N. Dorsano, M. R. Douglas, D. Dow, J. Downie, E. Downing, M. Dozieres, V. Draggoo, D. Drake, R. P. Drake, T. Drake, G. Dreifuerst, D. F. DuBois, P. F. DuBois, G. Dunham, R. Dylla-Spears, A. K. L. Dymoke-Bradshaw, B. Dzenitis, C. Ebbers, M. Eckart, S. Eddinger, D. Eder, D. Edgell, M. J. Edwards, P. Efthimion, J. H. Eggert, B. Ehrlich, P. Ehrmann, S. Elhadj, C. Ellerbee, N. S. Elliott, C. L. Ellison, F. Elsner, M. Emerich, K. Engelhorn, T. England, E. English, P. Epperson, R. Epstein, G. Erbert, M. A. Erickson, D. J. Erskine, A. Erlandson, R. J. Espinosa, C. Estes, K. G. Estabrook, S. Evans, A. Fabyan, J. Fair, R. Fallejo, N. Farmer, W. A. Farmer, M. Farrell, V. E. Fatherley, M. Fedorov, E. Feigenbaum, M. Feit, W. Ferguson, J. C. Fernandez, A. Fernandez-Panella, S. Fess, J. E. Field, C. V. Filip, J. R. Fincke, T. Finn, S. M. Finnegan, R. G. Finucane, M. Fischer, A. Fisher, J. Fisher, B. Fishler, D. Fittinghoff, P. Fitzsimmons, M. Flegel, K. A. Flippo, J. Florio, J. Folta, P. Folta, L. R. Foreman, C. Forrest, A. Forsman, J. Fooks, M. Foord, R. Fortner, K. Fournier, D. E. Fratanduono, N. Frazier, T. Frazier, C. Frederick, M. S. Freeman, J. Frenje, D. Frey, G. Frieders, S. Friedrich, D. H. Froula, J. Fry, T. Fuller, J. Gaffney, S. Gales, B. Le Galloudec, K. K. Le Galloudec, A. Gambhir, L. Gao, W. J. Garbett, A. Garcia, C. Gates, E. Gaut, P. Gauthier, Z. Gavin, J. Gaylord, M. Geissel, F. Génin, J. Georgeson, H. Geppert-Kleinrath, V. Geppert-Kleinrath, N. Gharibyan, J. Gibson, C. Gibson, E. Giraldez, V. Glebov, S. G. Glendinning, S. Glenn, S. H. Glenzer, S. Goade, P. L. Gobby, S. R. Goldman, B. Golick, M. Gomez, V. Goncharov, D. Goodin, P. Grabowski, E. Grafil, P. Graham, J. Grandy, E. Grasz, F. Graziani, G. Greenman, J. A. Greenough, A. Greenwood, G. Gregori, T. Green, J. R. Griego, G. P. Grim, J. Grondalski, S. Gross, J. Guckian, N. Guler, B. Gunney, G. Guss, S. Haan, J. Hackbarth, L. Hackel, R. Hackel, C. Haefner, C. Hagmann, K. D. Hahn, S. Hahn, B. J. Haid, B. M. Haines, B. M. Hall, C. Hall, G. N. Hall, M. Hamamoto, S. Hamel, C. E. Hamilton, B. A. Hammel, J. H. Hammer, G. Hampton, A. Hamza, A. Handler, S. Hansen, D. Hanson, R. Haque, D. Harding, E. Harding, J. D. Hares, D. B. Harris, J. A. Harte, E. P. Hartouni, R. Hatarik, S. Hatchett, A. A. Hauer, M. Havre, R. Hawley, J. Hayes, J. Hayes, S. Hayes, A. Hayes-Sterbenz, C. A. Haynam, D. A. Haynes, D. Headley, A. Heal, J. E. Heebner, S. Heerey, G. M. Heestand, R. Heeter, N. Hein, C. Heinbockel, C. Hendricks, M. Henesian, J. Heninger, J. Henrikson, E. A. Henry, E. B. Herbold, M. R. Hermann, G. Hermes, J. E. Hernandez, V. J. Hernandez, M. C. Herrmann, H. W. Herrmann, O. D. Herrera, D. Hewett, R. Hibbard, D. G. Hicks, D. Hill, K. Hill, T. Hilsabeck, D. E. Hinkel, D. D. Ho, V. K. Ho, J. K. Hoffer, N. M. Hoffman, M. Hohenberger, M. Hohensee, W. Hoke, D. Holdener, F. Holdener, J. P.

Holder, B. Holko, D. Holunga, J. F. Holzrichter, J. Honig, D. Hoover, D. Hopkins, L. Berzak Hopkins, M. Hoppe, M. L. Hoppe, J. Horner, R. Hornung, C. J. Horsfield, J. Horvath, D. Hotaling, R. House, L. Howell, W. W. Hsing, S. X. Hu, H. Huang, J. Huckins, H. Hui, K. D. Humbird, J. Hund, J. Hunt, O. A. Hurricane, M. Hutton, K. H.-K. Huynh, L. Inandan, C. Iglesias, I. V. Igumenshchev, N. Izumi, M. Jackson, J. Jackson, S. D. Jacobs, G. James, K. Jancaitis, J. Jarboe, L. C. Jarrott, D. Jasion, J. Jaquez, J. Jeet, A. E. Jenei, J. Jensen, J. Jimenez, R. Jimenez, D. Jobe, Z. Johal, H. M. Johns, D. Johnson, M. A. Johnson, M. Gatu Johnson, R. J. Johnson, S. Johnson, S. A. Johnson, T. Johnson, K. Jones, O. Jones, M. Jones, R. Jorge, H. J. Jorgenson, M. Julian, B. I. Jun, R. Jungquist, J. Kaae, N. Kabadi, D. Kaczala, D. Kalantar, K. Kangas, V. V. Karasiev, M. Karasik, V. Karpenko, A. Kasarky, K. Kasper, R. Kauffman, M. I. Kaufman, C. Keane, L. Keaty, L. Kegelmeyer, P. A. Keiter, P. A. Kellett, J. Kellogg, J. H. Kelly, S. Kemic, A. J. Kemp, G. E. Kemp, G. D. Kerbel, D. Kershaw, S. M. Kerr, T. J. Kessler, M. H. Key, S. F. Khan, H. Khater, C. Kiikka, J. Kilkenny, Y. Kim, Y.-J. Kim, J. Kimko, M. Kimmel, J. M. Kindel, J. King, R. K. Kirkwood, L. Klaus, D. Klem, J. L. Kline, J. Klingmann, G. Kluth, P. Knapp, J. Knauer, J. Knipping, M. Knudson, D. Kobs, J. Koch, T. Kohut, C. Kong, J. M. Koning, P. Koning, S. Konior, H. Kornblum, L. B. Kot, B. Kozioziemski, M. Kozlowski, P. M. Kozlowski, J. Krammen, N. S. Krasheninnikova, B. Kraus, W. Krauser, J. D. Kress, A. L. Kritcher, E. Krieger, J. J. Kroll, W. L. Kruer, M. K. G. Kruse, S. Kucheyev, M. Kumbera, S. Kumpan, J. Kunimune, B. Kustowski, T. J. T. Kwan, G. A. Kyrala, S. Laffite, M. Lafon, K. LaFortune, B. Lahmann, B. Lairson, O. L. Landen, J. Langenbrunner, L. Lagin, T. Land, M. Lane, D. Laney, A. B. Langdon, S. H. Langer, A. Langro, N. E. Lanier, T. E. Lanier, D. Larson, B. F. Lasinski, D. Lassle, D. LaTray, G. Lau, N. Lau, C. Laumann, A. Laurence, T. A. Laurence, J. Lawson, H. P. Le, R. R. Leach, L. Leal, A. Leatherland, K. LeChien, B. Lechleiter, A. Lee, M. Lee, T. Lee, R. J. Leeper, E. Lefebvre, J.-P. Leidinger, B. LeMire, R. W. Lemke, N. C. Lemos, S. Le Pape, R. Lerche, S. Lerner, S. Letts, K. Levedahl, T. Lewis, C. K. Li, H. Li, J. Li, W. Liao, Z. M. Liao, D. Liedahl, J. Liebman, G. Lindford, E. L. Lindman, J. D. Lindl, H. Loey, R. A. London, F. Long, E. N. Loomis, F. E. Lopez, H. Lopez, E. Losbanos, S. Loucks, R. Lowe-Webb, E. Lundgren, A. P. Ludwigsen, R. Luo, J. Lusk, R. Lyons, T. Ma, Y. Macallop, M. J. MacDonald, B. J. MacGowan, J. M. Mack, A. J. Mackinnon, S. A. MacLaren, A. G. MacPhee, G. R. Magelssen, J. Magoon, R. M. Malone, T. Malsbury, R. Managan, R. Mancini, K. Manes, D. Maney, D. Manha, O. M. Mannion, A. M. Manuel, E. Mapoles, G. Mara, T. Marcotte, E. Marin, M. M. Marinak, C. Mariscal, D. A. Mariscal, E. F. Mariscal, E. V. Marley, J. A. Marozas, R. Marquez, C. D. Marshall, F. J. Marshall, M. Marshall, S. Marshall, J. Marticorena, D. Martinez, I. Maslennikov, D. Mason, R. J. Mason, L. Masse, W. Massey, P.-E. Masson-Laborde, N. D. Masters, D. Mathisen, E. Mathison, J. Matone, M. J. Matthews, C. Mattoon, T. R. Mattsson, K. Matzen, C. W. Mauche, M. Mauldin, T. McAbee, M. McBurney, T. Mccarville, R. L. McCrory, A. M. McEvoy, C. McGuffey, M. Mcinnis, P. McKenty, M. S. McKinley, J. B. McLeod, A. McPherson, B. Mcquillan, M. Meamber, K. D. Meaney, N. B. Meezan, R. Meissner, T. A. Mehlhorn, N. C. Mehta, J. Menapace, F. E. Merrill, B. T. Merritt, E. C. Merritt, D. D. Meyerhofer, S. Mezyk, R. J. Mich, P. A. Michel, D. Milam, C. Miller, D. Miller, D. S. Miller, E. Miller, E. K. Miller, J. Miller, M. Miller, P. E. Miller, T. Miller, W. Miller, V. Miller-Kamm, M. Millot, J. L. Milovich, P. Minner, J.-L. Miquel, S. Mitchell, K. Molvig, R. C. Montesanti, D. S. Montgomery, M. Monticelli, A. Montoya, J. D. Moody, A. S. Moore, E. Moore, M. Moran, J. C. Moreno, K. Moreno, B. E. Morgan, T. Morrow, J. W. Morton, E. Moses, K. Moy, R. Muir, M. S. Murillo, J. E. Murray, J. R. Murray, D. H. Munro, T. J. Murphy, F. M. Munteanu, J. Nafziger, T. Nagayama, S. R. Nagel, R. Nast, R. A. Negres, A. Nelson, D. Nelson, J. Nelson, S. Nelson, S. Nemethy, P. Neumayer, K. Newman, M. Newton, H. Nguyen, J.-M. G. Di Nicola, P. Di Nicola, C. Niemann, A. Nikroo, P. M. Nilson, A. Nobile, V. Noorai, R. Nora, M. Norton, M. Nostrand, V. Note, S. Novell, P. F. Nowak, A. Nunez, R. A. Nyholm, M. O'Brien, A. Oceguera, J. A. Oertel, J. Okui, B. Olejniczak, J. Oliveira, P. Olsen, B. Olson, K. Olson, R. E. Olson, Y. P. Opachich, N. Orsi, C. D. Orth, M. Owen, S. Padalino, E. Padilla, R. Paguio, S. Paguio, J. Paisner, S. Pajoom, A. Pak, S. Palaniyappan, K. Palma, T. Pannell, F. Papp, D. Paras, T. Parham, H.-S. Park, A. Pasternak, S. Patankar, M. V. Patel, P. K. Patel, R. Patterson, S. Patterson, B. Paul, M. Paul, E. Pauli, O. T. Pearce, J. Pearcy, B. Pedrotti, A. Peer, L. J. Pelz, B. Penetrante, J. Penner, A. Perez, L. J. Perkins, E. Pernice, T. S. Perry, S. Person, D. Petersen, T. Petersen, D. L. Peterson, E. B. Peterson, J. E. Peterson, J. L. Peterson, K. Peterson, R. R. Peterson, R. D. Petrasso, F. Philippe, T. J. Phipps, E. Piceno, Y. Ping, L. Pickworth, J. Pino, R. Plummer, G. D. Pollack, S. M. Pollaine, B. B. Pollock, D. Ponce, J. Ponce, J. Pontelandolfo, J. L. Porter, J. Post, O. Poujade, C. Powell, H. Powell, G. Power, M. Pozulp, M. Prantil, M. Prasad, S. Pratuch, S. Price, K. Primdahl, S. Prisbrey, R. Procassini, A. Pruyne, B. Pudliner, S. R. Qiu, K. Quan, M. Quinn, J. Quintenz, P. B. Radha, F. Rainer, J. E. Ralph, K. S. Raman, R. Raman, P. Rambo, S. Rana, A. Randewich, D. Rardin, M. Ratledge, N. Ravelo, F. Ravizza, M. Rayce, A. Raymond, B. Raymond, B. Reed, C. Reed, S. Regan, B. Reichelt, V. Reis, S. Reisdorf, V. Rekow, B. A. Remington, A. Rendon, W. Requieron, M. Rever, H. Reynolds, J. Reynolds, J. Rhodes, M. Rhodes, M. C. Richardson, B. Rice, N. G. Rice, R. Rieben, A. Rigatti, S. Riggs, H. G. Rinderknecht, K. Ring, B. Riordan, R. Riquier, C. Rivers, D. Roberts, V. Roberts, G. Robertson, H. F. Robey, J. Robles, P. Rocha, G. Rochau, J. Rodriguez, S. Rodriguez, M. Rosen, M. Rosenberg, G. Ross, J. S. Ross, P. Ross, J. Rouse, D. Rovang, A. M. Rubenchik, M. S. Rubery, C. L. Ruiz, M. Rushford, B. Russ, J. R. Rygg, B. S. Ryujin, R. A. Sacks, R. F. Sacks, K. Saito, T. Salmon, J. D. Salmonson, J. Sanchez, S. Samuelson, M. Sanchez, C. Sangster, A. Saroyan, J. Sater, A. Satsangi, S. Sauers, R. Saunders, J. P. Sauppe, R. Sawicki, D. Sayre, M. Scanlan, K. Schaffers, G. T. Schappert, S. Schiaffino, D. J. Schlossberg, D. W. Schmidt, M. J. Schmitt, D. H. G. Schneider, M. B. Schneider, R. Schneider, M. Schoff, M. Schollmeier, M. Schölmerich, C. R.

Schroeder, S. E. Schrauth, H. A. Scott, I. Scott, J. M. Scott, R. H. H. Scott, C. R. Scullard, T. Sedillo, F. H. Seguin, W. Seka, J. Senecal, S. M. Sepke, L. Seppala, K. Sequoia, J. Severyn, J. M. Sevier, N. Sewell, S. Seznec, R. C. Shah, J. Shamlian, D. Shaughnessy, M. Shaw, R. Shaw, C. Shearer, R. Shelton, N. Shen, M. W. Sherlock, A. I. Shestakov, E. L. Shi, S. J. Shin, N. Shingleton, W. Shmayda, M. Shor, M. Shoup, C. Shuldberg, L. Siegel, F. J. Silva, A. N. Simakov, B. T. Sims, D. Sinars, P. Singh, H. Sio, K. Skulina, S. Skupsky, S. Slutz, M. Sluyter, V. A. Smalyuk, D. Smauley, R. M. Smeltser, C. Smith, I. Smith, J. Smith, L. Smith, R. Smith, R. Sohn, S. Sommer, C. Sorce, M. Sorem, J. M. Soures, M. L. Spaeth, B. K. Spears, S. Speas, D. Speck, R. Speck, J. Spears, T. Spinka, P. T. Springer, M. Stadermann, B. Stahl, J. Stahoviak, L. G. Stanton, R. Steele, W. Steele, D. Steinman, R. Stemke, R. Stephens, S. Sterbenz, P. Sterne, D. Stevens, J. Stevers, C. B. Still, C. Stoeckl, W. Stoeffl, J. S. Stolken, C. Stolz, E. Storm, G. Stone, S. Stoupin, E. Stout, I. Stowers, R. Strauser, H. Streckart, J. Streit, D. J. Strozzi, T. Suratwala, G. Sutcliffe, L. J. Suter, S. B. Sutton, V. Svidzinski, G. Swadling, W. Sweet, A. Szoke, M. Tabak, M. Takagi, A. Tambazidis, V. Tang, M. Taranowski, L. A. Taylor, S. Telford, W. Theobald, M. Thi, A. Thomas, C. A. Thomas, I. Thomas, R. Thomas, I. J. Thompson, A. Thongstisubskul, C. B. Thorsness, G. Tietbohl, R. E. Tipton, M. Tobin, N. Tomlin, R. Tommasini, A. J. Toreja, J. Torres, R. P. J. Town, S. Townsend, J. Trenholme, A. Trivelpiece, C. Trosseille, H. Truax, D. Trummer, S. Trummer, T. Truong, D. Tubbs, E. R. Tubman, T. Tunnell, D. Turnbull, R. E. Turner, M. Ulitsky, R. Upadhye, J. L. Vaher, P. VanArsdall, D. VanBlarcom, M. Vandenboomgaerde, R. VanQuinlan, B. M. Van Wonterghem, W. S. Varnum, A. L. Velikovich, A. Vella, C. P. Verdon, B. Vermillion, S. Vernon, R. Vesey, J. Vickers, R. M. Vignes, M. Visosky, J. Vocke, P. L. Volegov, S. Vonhof, R. Von Rotz, H. X. Vu, M. Vu, D. Wall, J. Wall, R. Wallace, B. Wallin, D. Walmer, C. A. Walsh, C. F. Walters, C. Waltz, A. Wan, A. Wang, Y. Wang, J. S. Wark, B. E. Warner, J. Watson, R. G. Watt, P. Watts, J. Weaver, R. P. Weaver, S. Weaver, C. R. Weber, P. Weber, S. V. Weber, P. Wegner, B. Welday, L. Welser-Sherrill, K. Weiss, K. Widmann, G. F. Wheeler, W. Whistler, R. K. White, H. D. Whitley, P. Whitman, M. E. Wickett, C. Widmayer, J. Wiedwald, R. Wilcox, S. Wilcox, C. Wild, B. H. Wilde, C. H. Wilde, K. Wilhelmsen, M. D. Wilke, H. Wilkens, P. Wilkins, S. C. Wilks, E. A. Williams, G. J. Williams, W. Williams, W. H. Williams, D. C. Wilson, B. Wilson, E. Wilson, R. Wilson, S. Winters, J. Wisoff, M. Wittman, J. Wolfe, A. Wong, K. W. Wong, L. Wong, N. Wong, R. Wood, D. Woodhouse, J. Woodruff, D. T. Woods, S. Woods, B. N. Woodworth, E. Wooten, A. Wootton, K. Work, J. B. Workman, J. Wright, M. Wu, C. Wuest, F. J. Wysocki, H. Xu, M. Yamaguchi, B. Yang, S. T. Yang, J. Yatabe, C. B. Yeamans, B. C. Yee, S. A. Yi, L. Yin, B. Young, C. S. Young, C. V. Young, P. Young, K. Youngblood, R. Zacharias, G. Zagaris, N. Zaitseva, F. Zaka, F. Ze, B. Zeiger, M. Zika, G. B. Zimmerman, T. Zobrist, J. D. Zuegel, and A. B. Zylstra (Indirect Drive ICF Collaboration), Phys. Rev. Lett. **129**, 075001 (2022).

[2] A. L. Kritcher, A. B. Zylstra, D. A. Callahan, O. A. Hurricane, C. R. Weber, D. S. Clark, C. V. Young, J. E. Ralph, D. T. Casey, A. Pak, O. L. Landen, B. Bachmann, K. L. Baker, L. Berzak Hopkins, S. D. Bhandarkar, J. Biener, R. M. Bionta, N. W. Birge, T. Braun, T. M. Briggs, P. M. Celliers, H. Chen, C. Choate, L. Divol, T. Döppner, D. Fittinghoff, M. J. Edwards, M. Gatu Johnson, N. Gharibyan, S. Haan, K. D. Hahn, E. Hartouni, D. E. Hinkel, D. D. Ho, M. Hohenberger, J. P. Holder, H. Huang, N. Izumi, J. Jeet, O. Jones, S. M. Kerr, S. F. Khan, H. Geppert Kleinrath, V. Geppert Kleinrath, C. Kong, K. M. Lamb, S. Le Pape, N. C. Lemos, J. D. Lindl, B. J. MacGowan, A. J. Mackinnon, A. G. MacPhee, E. V. Marley, K. Meaney, M. Millot, A. S. Moore, K. Newman, J.-M. G. Di Nicola, A. Nikroo, R. Nora, P. K. Patel, N. G. Rice, M. S. Rubery, J. Sater, D. J. Schlossberg, S. M. Sepke, K. Sequoia, S. J. Shin, M. Stadermann, S. Stoupin, D. J. Strozzi, C. A. Thomas, R. Tommasini, C. Trosseille, E. R. Tubman, P. L. Volegov, C. Wild, D. T. Woods, and S. T. Yang, Phys. Rev. E **106**, 025201 (2022).

[3] A. B. Zylstra, A. L. Kritcher, O. A. Hurricane, D. A. Callahan, J. E. Ralph, D. T. Casey, A. Pak, O. L. Landen, B. Bachmann, K. L. Baker, L. Berzak Hopkins, S. D. Bhandarkar, J. Biener, R. M. Bionta, N. W. Birge, T. Braun, T. M. Briggs, P. M. Celliers, H. Chen, C. Choate, D. S. Clark, L. Divol, T. Döppner, D. Fittinghoff, M. J. Edwards, M. Gatu Johnson, N. Gharibyan, S. Haan, K. D. Hahn, E. Hartouni, D. E. Hinkel, D. D. Ho, M. Hohenberger, J. P. Holder, H. Huang, N. Izumi, J. Jeet, O. Jones, S. M. Kerr, S. F. Khan, H. Geppert Kleinrath, V. Geppert Kleinrath, C. Kong, K. M. Lamb, S. Le Pape, N. C. Lemos, J. D. Lindl, B. J. MacGowan, A. J. Mackinnon, A. G. MacPhee, E. V. Marley, K. Meaney, M. Millot, A. S. Moore, K. Newman, J.-M. G. Di Nicola, A. Nikroo, R. Nora, P. K. Patel, N. G. Rice, M. S. Rubery, J. Sater, D. J. Schlossberg, S. M. Sepke, K. Sequoia, S. J. Shin, M. Stadermann, S. Stoupin, D. J. Strozzi, C. A. Thomas, R. Tommasini, C. Trosseille, E. R. Tubman, P. L. Volegov, C. R. Weber, C. Wild, D. T. Woods, S. T. Yang, and C. V. Young, Phys. Rev. E **106**, 025202 (2022).

[4] S. Le Pape, L. F. Berzak Hopkins, L. Divol, A. Pak, E. L. Dewald, S. Bhandarkar, L. R. Bennedetti, T. Bunn, J. Biener, J. Crippen, D. Casey, D. Edgell, D. N. Fittinghoff, M. Gatu-Johnson, C. Goyon, S. Haan, R. Hatarik, M. Havre, D. D.-M. Ho, N. Izumi, J. Jaquez, S. F. Khan, G. A. Kyrala, T. Ma, A. J. Mackinnon, A. G. MacPhee, B. J. MacGowan, N. B. Meezan, J. Milovich, M. Millot, P. Michel, S. R. Nagel, A. Nikroo, P. Patel, J. Ralph, J. S. Ross, N. G. Rice, D. Strozzi, M. Stadermann, P. Volegov, C. Yeamans, C. Weber, C. Wild, D. Callahan, and O. A. Hurricane, Phys. Rev. Lett. **120**, 245003 (2018).

[5] K. L. Baker, C. A. Thomas, D. T. Casey, S. Khan, B. K. Spears, R. Nora, T. Woods, J. L. Milovich, R. L. Berger, D. Strozzi, D. Clark, M. Hohenberger, O. A. Hurricane, D. A. Callahan, O. L. Landen, B. Bachmann, R. Benedetti, R. Bionta, P. M. Celliers, D. Fittinghoff, C. Goyon, G. Grim, R. Hatarik, N. Izumi, M. Gatu Johnson, G. Kyrala, T. Ma, M. Millot, S. R. Nagel, A. Pak, P. K. Patel, D. Turnbull, P. L. Volegov, and C. Yeamans, Phys. Rev. Lett. **121**, 135001 (2018).

[6] D. T. Casey, C. A. Thomas, K. L. Baker, B. K. Spears, M. Hohenberger, S. F. Khan, R. C. Nora, C. R. We-

ber, D. T. Woods, O. A. Hurricane, D. A. Callahan, R. L. Berger, J. L. Milovich, P. K. Patel, T. Ma, A. Pak, L. R. Benedetti, M. Millot, C. Jarrott, O. L. Landen, R. M. Bionta, B. J. MacGowan, D. J. Strozzi, M. Stadermann, J. Biener, A. Nikroo, C. S. Goyon, N. Izumi, S. R. Nagel, B. Bachmann, P. L. Volegov, D. N. Fittinghoff, G. P. Grim, C. B. Yeamans, M. Gatu Johnson, J. A. Frenje, N. Rice, C. Kong, J. Crippen, J. Jaquez, K. Kangas, and C. Wild, Physics of Plasmas **25**, 056308 (2018), https://doi.org/10.1063/1.5019741.

[7] R. L. Berger, C. A. Thomas, K. L. Baker, D. T. Casey, C. S. Goyon, J. Park, N. Lemos, S. F. Khan, M. Hohenberger, J. L. Milovich, D. J. Strozzi, M. A. Belyaev, T. Chapman, and A. B. Langdon, Phys. Plasmas **26**, 012709 (2019).

[8] A. B. Zylstra, A. L. Kritcher, O. A. Hurricane, D. A. Callahan, K. Baker, T. Braun, D. T. Casey, D. Clark, K. Clark, T. Döppner, L. Divol, D. E. Hinkel, M. Hohenberger, C. Kong, O. L. Landen, A. Nikroo, A. Pak, P. Patel, J. E. Ralph, N. Rice, R. Tommasini, M. Schoff, M. Stadermann, D. Strozzi, C. Weber, C. Young, C. Wild, R. P. J. Town, and M. J. Edwards, Phys. Rev. Lett. **126**, 025001 (2021).

[9] A. L. Kritcher, A. B. Zylstra, D. A. Callahan, O. A. Hurricane, C. Weber, J. Ralph, D. T. Casey, A. Pak, K. Baker, B. Bachmann, S. Bhandarkar, J. Biener, R. Bionta, T. Braun, M. Bruhn, C. Choate, D. Clark, J. M. Di Nicola, L. Divol, T. Doeppner, V. Geppert-Kleinrath, S. Haan, J. Heebner, V. Hernandez, D. Hinkel, M. Hohenberger, H. Huang, C. Kong, S. Le Pape, D. Mariscal, E. Marley, L. Masse, K. D. Meaney, M. Millot, A. Moore, K. Newman, A. Nikroo, P. Patel, L. Pelz, N. Rice, H. Robey, J. S. Ross, M. Rubery, J. Salmonson, D. Schlossberg, S. Sepke, K. Sequoia, M. Stadermann, D. Strozzi, R. Tommasini, P. Volegov, C. Wild, S. Yang, C. Young, M. J. Edwards, O. Landen, R. Town, and M. Herrmann, Physics of Plasmas **28**, 072706 (2021), https://doi.org/10.1063/5.0047841.

[10] J. Lindl, P. Amendt, R. L. Berger, S. G. Glendinning, S. H. Glenzer, S. Haan, R. L. Kauffman, O. Landen, and L. J. Suter, Phys. Plasmas **11**, 339 (2004).

[11] E. A. Williams, R. L. Berger, R. P. Drake, A. M. Rubenchik, B. S. Bauer, D. D. Mayerhofer, A. C. Gaeris, and T. W. Johnston, Phys. Plasmas **2**, 129 (1995).

[12] D. S. Clark, S. W. Haan, A. W. Cook, M. J. Edwards, B. A. Hammel, J. M. Koning, and M. M. Marinak, Physics of Plasmas **18**, 082701 (2011), https://doi.org/10.1063/1.3609834.

[13] D. E. Hinkel, L. F. Berzak Hopkins, T. Ma, J. E. Ralph, F. Albert, L. R. Benedetti, P. M. Celliers, T. Döppner, C. S. Goyon, N. Izumi, L. C. Jarrott, S. F. Khan, J. L. Kline, A. L. Kritcher, G. A. Kyrala, S. R. Nagel, A. E. Pak, P. Patel, M. D. Rosen, J. R. Rygg, M. B. Schneider, D. P. Turnbull, C. B. Yeamans, D. A. Callahan, and O. A. Hurricane, Phys. Rev. Lett. **117**, 225002 (2016).

[14] A. L. Kritcher, D. Clark, S. Haan, S. A. Yi, A. B. Zylstra, D. A. Callahan, D. E. Hinkel, L. F. Berzak Hopkins, O. A. Hurricane, O. L. Landen, S. A. MacLaren, N. B. Meezan, P. K. Patel, J. Ralph, C. A. Thomas, R. Town, and M. J. Edwards, Physics of Plasmas **25**, 056309 (2018), https://doi.org/10.1063/1.5018000.

[15] B. MacGowan, BAPS **63** (2018).

[16] J. E. Ralph, A. Kemp, N. B. Meezan, R. L. Berger, D. Strozzi, B. J. MacGowan, O. Landen, N. Lemos, M. Belyaev, M. Biener, D. A. Callahan, T. Chapman, L. Divol, D. E. Hinkel, J. Moody, A. Nikroo, O. Jones, S. Schiaffino, M. Stadermann, and P. Michel, Phys. Plasmas **28**, 072704 (2021).

[17] J.-L. Miquel, C. Lion, and P. Vivini, Journal of Physics: Conference Series **688**, 012067 (2016).

[18] C. Lion, Journal of Physics: Conference Series **244**, 012003 (2010).

[19] H. Vu, D. DuBois, and B. Bezzerides, Phys. Rev. Lett. **86**, 4306 (2001).

[20] R. L. Berger, S. Brunner, T. Chapman, L. Divol, C. H. Still, and E. J. Valeo, Phys. Plasmas **20**, 032107 (2013).

[21] P. W. Rambo, S. C. Wilks, and W. L. Kruer, Phys. Rev. Lett. **79**, 83 (1997).

[22] J. W. Banks, S. Brunner, R. L. Berger, and T. M. Tran, Phys. Plasmas **23**, 032108 (2016).

[23] J. W. Banks, S. Brunner, R. L. Berger, W. J. Arrighi, and T. M. Tran, Phys. Rev. E **96**, 043208 (2017).

[24] A. M. Dimits, J. W. Banks, R. L. Berger, S. Brunner, T. Chapman, D. Copeland, D. Ghosh, W. J. Arrighi, J. Hittinger, and I. Joseph, IEEE T. Plasma. Sci. **47**, 2074 (2019).

[25] J. W. Banks and J. A. F. Hittinger, IEEE T. Plasma. Sci. **38**, 2198 (2010).

[26] J. W. Banks, A. G. Odu, R. Berger, T. Chapman, W. Arrighi, and S. Brunner, SIAM Journal on Scientific Computing **41**, B953 (2019), https://doi.org/10.1137/19M1238551.

[27] S. Brunner and E. J. Valeo, Phys. Rev. Lett. **93**, 145003 (2004).

[28] S. Brunner, R. L. Berger, B. I. Cohen, L. Hausammann, and E. J. Valeo, Phys. Plasmas **21**, 102104 (2014).

[29] R. L. Berger, S. Brunner, J. W. Banks, B. I. Cohen, and B. J. Winjum, Phys. Plasmas **23**, 1234 (2015).

[30] T. Chapman, S. Brunner, J. W. Banks, R. L. Berger, B. Cohen, and E. A. Williams, Phys. Plasmas **21**, 042107 (2014).

[31] T. Chapman, R. L. Berger, B. I. Cohen, J. W. Banks, and S. Brunner, Phys. Rev. Lett. **119**, 055002 (2017).

[32] B. J. Albright, L. Yin, K. J. Bowers, and B. Bergen, Phys. Plasmas **23**, 032703 (2016).

[33] T. Chapman, R. L. Berger, S. Brunner, and E. A. Williams, Phys. Rev Lett **110**, 042107 (2013).

[34] R. L. Berger and E. J. Valeo, Phys. Plasmas **12**, 032104 (2005).

[35] B. A. Trubnikov, "Particle interactions in a fully ionized plasma," in *Reviews of Plasma Physics*, Reviews of Plasma Physics, Vol. 1 (M. A. Leontovich, Consultants Bureau, New York, 1965) p. 105.

[36] These relations are also in the NRL Plasma Formulary https://www.nrl.navy.mil/News-Media/Publications/nrl-plasma-formulary/.

[37] In Ref. 20, Eqns A3 and A4 are incorrect; Eqns. 2 and 3 are the correct equations.

[38] R. L. Berger, C. H. Still, E. A. Williams, and A. B. Langdon, Phys. Plasmas **5**, 4337 (1998).

[39] PF3D is a fluid simulation code that solves 3D paraxial wave equations for the laser, backscattered light, and ion acoustic waves. The waves are coupled via ponderomotive forces and scattering from IAW density perturbations. Inverse bremsstrahlung light wave absorption and Landau damping of the plasma waves are included.

[40] K. L. Baker, C. A. Thomas, D. T. Casey, S. F. Khan, B. K. Spears, R. C. Nora, D. T. Woods, J. L. Milovich,

R. L. Berger, D. J. Strozzi, D. Clark, M. Hohenberger, O. A. Hurricane, D. A. Callahan, O. L. Landen, B. Bachmann, L. R. Benedetti, R. M. Bionta, P. M. Celliers, D. N. Fittinghoff, C. S. Goyon, G. P. Grim, R. Hatarik, N. Izumi, M. G. Johnson, G. Kyrala, T. Ma, M. Millot, S. R. Nagel, A. Pak, P. K. Patel, D. Turnbull, P. L. Volegov, and C. B. Yeamans, Phys. Rev. Lett. **121**, 135001 (2018).

[41] D. T. Casey, C. A. Thomas, K. L. Baker, B. K. Spears, M. Hohenberger, S. F. Khan, R. C. Nora, C. R. Weber, D. T. Woods, O. A. Hurricane, D. A. Callahan, R. L. Berger, J. L. Milovich, P. K. Patel, T. Ma, A. Pak, L. R. Benedetti, M. Millot, C. Jarrott, O. L. Landen, R. M. Bionta, B. J. MacGowan, D. J. Strozzi, M. Stadermann, J. Biener, A. Nikroo, C. S. Goyon, N. Izumi, S. R. Nagel, B. Bachmann, P. L. Volegov, D. N. Fittinghoff, G. P. Grim, C. B. Yeamans, M. G. Johnson, J. A. Frenje, N. Rice, C. Kong, J. Crippen, J. Jaquez, Kangas, and C. Wild, Phys. Plasmas **25**, 056308 (2018).

[42] L. J. Babati, W. A. Farmer, R. L. Berger, M. A. Belyaev, T. Chapman, D. E. Hinkel, E. Kur, and E. A. Williams, AIP Advances **12**, 095005 (2022), https://doi.org/10.1063/5.0090057.

[43] H. A. Rose, Phys. Plasmas **12**, 012318 (2005).

[44] L. Yin, B. J. Albright, H. A. Rose, K. J. Bowers, B. Bergen, R. Kirkwood, D. E. Hinkel, A. B. Langdon, P. Michel, D. S. Montgomery, and J. L. Kline, Phys. Plasmas **19**, 056304 (2012).

[45] J. W. Banks, R. L. Berger, S. Brunner, B. I. Cohen, and J. A. F. Hittinger, Phys. Plasmas **18**, 052102 (2011).

[46] B. Winjum, R. L. Berger, T. Chapman, J. W. Banks, and S. Brunner, Phy. Rev. Lett. **111**, 115002 (2013).

[47] R. L. Dewar, Phys. Fluids **15**, 712 (1972).

[48] D. J. Strozzi, E. A. Williams, H. A. Rose, D. E. Hinkel, A. B. Langdon, and J. W. Banks, Physics of Plasmas **19**, 112306 (2012), https://doi.org/10.1063/1.4767644.

[49] E. A. Williams, B. I. Cohen, L. Divol, M. R. Dorr, J. A. Hittinger, D. E. Hinkel, A. B. Langdon, R. K. Kirkwood, D. H. Froula, and S. H. Glenzer, Phys. Plasmas **11**, 231 (2004).

[50] L. Divol, E. A. Williams, B. I. Cohen, A. B. Langdon, and B. F. Lasinski, in *Proceedings of the Third International Conference on Inertial Fusion Sciences and Applications (IFSA2003)* (2003).

[51] B. I. Cohen, E. A. Williams, and H. X. Vu, Phys. Plasmas **14**, 102707 (2007).

[52] C. Riconda, A. Heron, D. Pesme, S. Huller, V. T. Tikhonchuk, and F. Detering, Phys. Rev. Lett. **94**, 055003 (2005).

[53] C. Riconda, A. Heron, D. Pesme, S. Huller, V. T. Tikhonchuk, and F. Detering, Phys. Plasmas **12**, 112308 (2005).

[54] F. Detering, J.-C. Adam, A. Heron, S. Huller, P.-E. Masson-Laborde, and D. Pesme, J. Phys (2005).

[55] R. Belaouar, V. T. Tikhonchuk, T. Colin, and G. Gallice, Plasma Physics and Controlled Fusion **49**, 969 (2007).

[56] If the dynamics of the plasma response are negligible, ponderomotive self-focusing is mathematically similar to light self-focusing in glass where the index of refraction is modified by the Kerr nonlinear index n_2 to be dependent of the light intensity, $\tilde{n} = \tilde{n}_0 + n_2 I$.